Neurotherapeutics 22 (2025) e00544

Contents lists available at ScienceDirect

Neurotherapeutics

journal homepage: www.sciencedirect.com/journal/neurotherapeutics

Original Article

Fasudil inhibits α-synuclein aggregation through ROCK-inhibition-mediated mechanisms

Lucia Lage [a], Ana I. Rodriguez-Perez [a,b], Jose Luis Labandeira-Garcia [a,b,*], Antonio Dominguez-Meijide [a,b,**]

[a] Cellular and Molecular Neurobiology of Parkinson's Disease, Research Center for Molecular Medicine and Chronic Diseases (CIMUS), IDIS, University of Santiago de Compostela, Santiago de Compostela, Spain
[b] Networking Research Center on Neurodegenerative Diseases (CIBERNED), Spain

ARTICLE INFO

Keywords:
Alpha-synuclein
Angiotensin
Neurodegeneration
Neuroinflammation
Parkinson
Rho-kinase

ABSTRACT

ROCK inhibitors such as fasudil protected against dopaminergic degeneration and other neurodegenerative processes in several experimental models through inhibition of neuroinflammation and activation of survival signaling pathways, and clinical trials have been initiated. More recently, fasudil has been suggested to inhibit α-synuclein aggregation. However, this is controversial, particularly if it is a consequence of direct binding of the fasudil molecule to α-synuclein. We studied the mechanisms involved in the effects of fasudil on α-synuclein aggregation using the α-synuclein-T/V5-synphilin-1 model. Molecule-molecule interactions were studied using real time quaking inducing conversion (RT-QuiC). Fasudil decreased the number of cells with inclusions and the size of inclusions in dopaminergic neurons and glial cells, and inhibited α-synuclein aggregation and microglial endocytosis of aggregates. These changes were not due to changes in α-synuclein protein expression or phosphorylation and were related to ROCK inhibition rather than direct interaction with α-synuclein, as confirmed with a second ROCK inhibitor (Y27632) and ROCK gene silencing. We observed that ROCK inhibition downregulates several factors that are known to promote α-synuclein aggregation such as NADPH-oxidase-derived oxidative stress, intracellular calcium increase, and α-synuclein endocytosis, and promotes autophagy. The present results support that fasudil is a useful drug against Parkinson's disease progression. In addition to other reported neuroprotective properties, fasudil inhibits α-synuclein aggregation and microglial endocytosis of aggregates, which enhances the microglial inflammatory response. The effects of fasudil are mostly related to ROCK inhibition, which we have shown using two structurally different ROCK inhibitors and knockdown data, and further supported by using RT-QuiC.

Introduction

Parkinson's disease (PD) is the second most common neurodegenerative disease, and its prevalence is increasing as the global population ages [1,2]. Although the initial trigger of idiopathic PD remains to be clarified and, PD is probably a multifactorial process, and oxidative stress, neuroinflammation and the presence of protein aggregates termed Lewy bodies have been identified as major mechanisms involved in the disease progression [3]. One of the characteristics of Lewy bodies is the presence of misfolded forms of α-synuclein [4]. α-Synuclein is a small intrinsically disordered protein that has a 140-residue sequence, whose function is still unclear [5,6]. But, as α-synuclein transiently binds to lipid membranes and free fatty acids via its *N*-terminal domain [7], it may be related to neurotransmitter release, clustering of synaptic vesicles, and vesicle-trafficking [5,6].

Rho kinase (ROCK) is the major downstream effector of the small GTP-binding protein RhoA, a member of the Rho family [8,9]. Several studies, using *in vitro* and *in vivo* models of PD, have shown that ROCK inhibitors such as fasudil and Y27632, protect against dopaminergic neuron cell death [10–13] and other neurodegenerative processes [14,15]. A major mechanism of neuroprotection is the inhibition of the microglial neuroinflammatory response [10,11,13]; however, it has also been suggested that the neuroprotective effects may be related to the activation of survival signaling pathways such as MAPK and Akt by ROCK

* Corresponding author.
** Corresponding author.
E-mail addresses: joseluis.labandeira@usc.es (J.L. Labandeira-Garcia), antonio.meijide@usc.es (A. Dominguez-Meijide).

https://doi.org/10.1016/j.neurot.2025.e00544
Received 9 June 2024; Received in revised form 27 January 2025; Accepted 27 January 2025

inhibition [12]. It has been suggested that ROCK may also be involved in α-synuclein aggregation, which may be counteracted by treatment with ROCK inhibitors such as fasudil [16,17]. However, other studies have suggested that the inhibitory effects of fasudil on α-synuclein aggregation are related to the direct binding of the molecule to α-synuclein, which inhibits its aggregation rate, than due to ROCK inhibition [18,19], and that other ROCK inhibitors may be not effective [19]. Fasudil has been suggested for neuroprotective treatment of PD and other neurodegenerative diseases [14,15] and for treatment of dyskinesias in PD [20], and some clinical trials have been initiated [21,22]. Therefore, the mechanisms involved in the effects of fasudil, particularly the effects on aggregation require further clarification. *In vitro,* we induced α-synuclein aggregates by over-expression α-synuclein in different types of cells, including dopaminergic neuronal cells, astrocytes, and microglial cells. We also induced an increase in the aggregation by treatment of cultures with angiotensin II (AngII) [23]. *In vivo*, α-synuclein aggregation was induced in mice treated with MPTP [23–25]. In these models, we studied the mechanisms involved in the effects of fasudil and ROCK inhibition on α-synuclein aggregation. In addition, possible direct effects of fasudil on α-synuclein aggregation due to molecule-molecule interactions were studied using real time quaking inducing conversion (RT-QuiC).

Materials and methods

Experimental design

Several *in vitro* and *in vivo* experiments were designed to study the effects of fasudil on α-synuclein aggregation. For the *in vitro* experiments (summarized in Fig. 1), we used dopaminergic neuron and major glial cell lines involved in dopaminergic degeneration: N27 dopaminergic neuronal cells, C6 astroglial cells, and HMC3 human microglial cells. In addition, human kidney HEK293 cells were used as a positive control for transfection and as a negative control for the effects of AngII, because they have a very high transfection efficiency and they do not express AT1 neither AT2 receptors [26,27]. In the *in vitro* experiments, we studied the effects of the ROCK inhibitor fasudil and the activation of the AngII/AT1 axis on α-synuclein aggregation using four experimental groups: untreated control cells, cells treated with AngII, cells treated with fasudil, and cells treated with AngII and fasudil. In these experimental groups, we assessed changes in the presence, quantity and size of aggregates using an α-synuclein aggregation model termed α-synuclein-T/V5-synphilin-1 (SynT/Sph1); this model has been already used for the assessment of the effects of different drugs on α-synuclein aggregation [28–30]. The original plasmids were kindly donated by Dr. Tiago Outeiro, and new clones were prepared in our lab according to published protocols [31]. In this model, cells transfected with SynT and V5-SPH-1 plasmids express a certain number of aggregate-like structures termed inclusions, with similar structure to Lewy bodies [23]. We used this assay model because it has been extensively characterized. It has been shown that the changes in the *C*-terminal fragment of α-synuclein do not influence substantially the local conformational propensities adopted by untagged α-synuclein. Furthermore, chemical characterization of this cellular model shows impaired α-synuclein association to membranes and lipids, so it is unlikely that it may model lipid associated α-synuclein aggregation [32,33]. Only some *N*-terminal alterations could be observed in SynT and these, together with the hindrance of the *C*-terminus, could be responsible for the decreased membrane SynT binding capacity [33], and aggregation is due to intramolecular contacts between the *C*- and *N*- terminus [34]. It has been previously observed that Seed Amyloid Amplification (SAA) of purified recombinant SynT (i.e. the molecule alone) does not lead to aggregation [33]. However, previous studies have shown that the inclusions obtained in different cell models are positive for ThS binding [23,30], indicating beta-sheet aggregation. In addition to this, SAA amplification of cell lysates from EGFP-tagged synuclein show α-synuclein aggregation [35], further pointing to *in vivo* beta-sheet aggregation. In summary, inside cells, SynT leads to beta-sheet aggregation like that observed in SAA with monomeric recombinant α-synuclein. To confirm that the effects of fasudil on α-synuclein aggregation were related to ROCK inhibition and were also produced in an *in vivo* model, we induced aggregation of α-synuclein in mice by treatment with MPTP as detailed elsewhere [23–25]. In a recent study [23], we characterized the ThS-positive signals by different types of Western blot, including PSer129 in mice, and by immunofluorescence. Three treatment groups were established: the first group consisted of mice treated with vehicle solution. The second group consisted of mice treated with MPTP. Finally, the third group consisted of mice treated with MPTP plus the ROCK inhibitor Y27632 [36]. Brains were extracted and then processed for α-synuclein immunohistochemistry and aggregation using thioflavin S-staining (ThS). Image analysis was performed in the brain preparations as detailed below.

In another set of *in vitro* experiments, we studied possible mechanisms responsible for the effects of fasudil on α-synuclein aggregation. First, we studied by Western blot (WB) if changes in levels of α-synuclein expression or phosphorylation may be responsible for the effects of fasudil. In these experiments, and to assess transfection levels, we used a VN-α-synuclein/α-synuclein-VC BiFC technique as described in our previous work [23]. Second, we analyzed possible direct effects of fasudil on α-synuclein aggregation by molecule-molecule interactions, performing a technique known as real-time quaking-inducing conversion (RT-QuiC). In this procedure, a mix of fasudil, monomeric recombinant α-synuclein and α-synuclein pre-formed fibrils (PFFs) were subjected to subsequent cycles of shaking (quaking) and repose to induce α-synuclein aggregation over time. Aggregation levels were measured in real time by emission fluorescence of Thioflavin T (ThT). Molecule-molecule interactions between fasudil and α-synuclein lead to changes in ThT fluorescence, which imply changes in aggregation kinetics. PFFs, produced in our lab as detailed below, were added as seeds for aggregation, acting as aggregation nuclei, speeding the reaction. Third, we studied the effects of fasudil on α-synuclein aggregation induced by treatment with PFFs on neuronal cells; for this, protein extracts from cells treated with fasudil and/or PFFs were subjected to RT-QuiC. Fourth, we studied the effects of fasudil on α-synuclein incorporation by microglial cells. We performed direct co-cultures, adding HMC3 human microglial cells to N27 neuronal cells expressing α-synuclein tagged to EGFP. Incorporation of α-synuclein was directly assessed first, by identifying HMC3 cells by immunocytochemistry in combination with flow cytometry, and then identifying which ones have incorporated EGFP-tagged α-synuclein, also by flow cytometry. Fifth, we studied the effects of ROCK gene silencing (SiRNA) on α-synuclein aggregation. For this, four experimental groups were established: untreated control cells, cells treated with AngII, cells treated with a ROCK SiRNA, and cells treated with AngII and a ROCK SiRNA. Finally, we studied if fasudil and the inhibition of ROCK activity with a different specific ROCK inhibitor (Y27632) affected cell mechanisms that are known to be involved in α-synuclein aggregation such as NADPH-oxidase (Nox) activity, intracellular calcium increase and autophagy, which were analyzed using already established assays based on colorimetry (for Nox activity), live cell imaging (for calcium), and WB and flow cytometry (for autophagy).

Cell culture and treatment

Dulbecco's modified Eagle medium (DMEM; 10-013-CV, Falcon Corning) with 10 % inactivated Fetal Bovine Serum (FBSi), 1 % fungizone and 1 % penicillin/streptomycin was used for the culture of human microglial (HMC3) and embryonic kidney (HEK293) cells. A 1:1 mixture of DMEM and Ham's F12 medium (10-092-CV, Falcon Corning) with 10 % FBS, 1 % fungizone and 1 % penicillin/streptomycin was used for the culture of C6 astroglial rat cells. Roswell Park Memorial Institute (RPMI) medium (R8758-1640) supplemented with 10 % FBS, 1 % fungizone, and 1 % penicillin/streptomycin was used for the culture of N27 neuronal cells. All cell lines were kept in a humidified incubator at 37 °C and with 5 % CO_2.

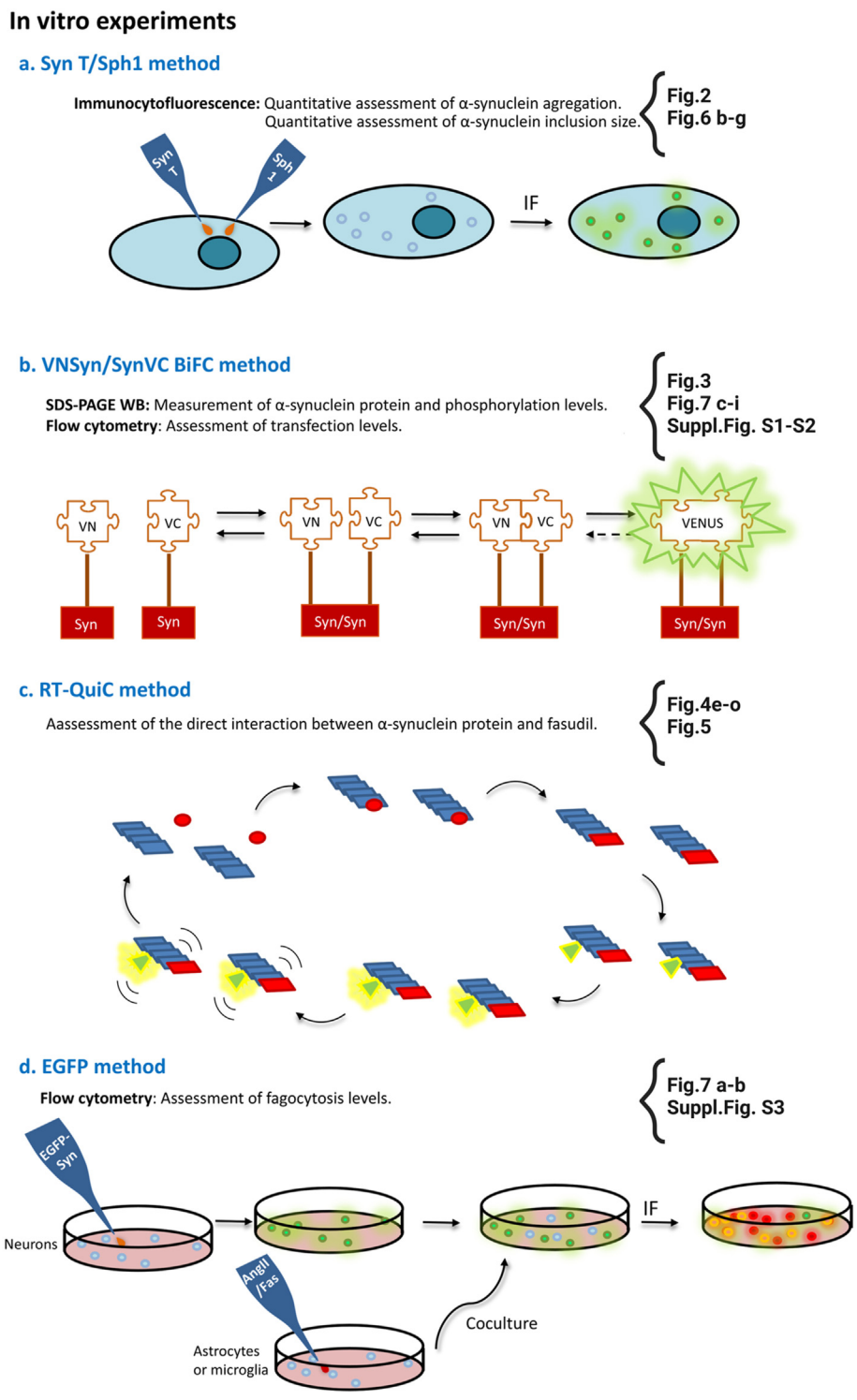

Fig. 1. Experimental design and schematic representation of the *in vitro* experiments. **(a)**: Schematic representation of the α-synuclein-T/Synphilin-1 method. Co-expression of SynT and V5-Sph-1 leads to the formation of inclusions that can be observed after immunofluorescence. **(b)**: Schematic representation of the VN-α-synuclein/α-synuclein-VC BiFC technique. α-synuclein tagged to the VN fragment of venus interacts with α-synuclein tagged to the VC fragment of venus leading to fluorescence. **(c)**: Schematic representation of the RT-QuiC amplification. Small α-synuclein aggregates will break after quaking, creating nucleation centers (seeds) that will incorporate monomeric α-synuclein, leading to the formation of bigger aggregates. ThT binds to aggregates of a certain size, changing its conformation and leading to fluorescence emission. **(d)**: Schematic representation of the incorporation of EGFP-tagged α-synuclein into microglia. AngII or AngII plus fasudil-treated microglial cells are co-cultured with neuron cells that express EGFP-tagged α-synuclein. EGFP-tagged α-synuclein is then incorporated into microglia, which is then identified by immunofluorescence and flow cytometry.

Twenty-four hours before transfection, approximately 100,000 cells were plated per well in a 12-well plate (Falcon, reference 353043). For HEK293, N27 and C6 cell lines transfection was performed with TRANSIT-X2 transfection reagent (Mirus Bio, Madison, USA) according to manufacturer's instructions. In brief: 2 µl of TRANSIT-X2 and 1 µg of total DNA were added to 100 µl of DMEM and incubated for 20 min at room temperature in the dark. The resulting mixture was added dropwise to the cells, and the plate was gently rocked. For HMC3 cells, transfection was performed with magnetic nanoparticles by using Glial Mag transfection reagent (OZBioscience, GL00500) according to the following protocol: 3.5 µl of Glial Mag and 1 µg of total DNA were added to 100 µl of DMEM and incubated for 30 min at room temperature. Immediately after this time, 3 µl of Glial Boost (OZBioscience, GL00500) for each µg of DNA were added to the mix. The resulting mixture was added dropwise to the cells, and the plate was gently rocked and put on top of a Super Magnetic Plate (OZBioscience, MF10000) for 45 min at room temperature to improve the introduction of the DNA into the cells. To avoid possible effects of fasudil on plasmid internalization (see below), treatments were performed as follow: Forty-eight hours after transfection, cells were fed with fresh medium, and 20 µM of fasudil

monohydrochloride salt (LC laboratories. F4660) or 30 μM of Y27632 (Merck, SCM075) were added dropwise. Cells were treated with 100 nM AngII (Sigma Aldrich, A9525) 30 min after fasudil or Y27632 treatment. Cells were treated again 24 and 48 h later and were kept in an incubator at 37 °C and 5 % CO_2.

To study the effect of fasudil on α-synuclein aggregation induced by treatment with PFFs, N27 cells were seeded at 200,000 cells per well in a 6-well plate. Twenty-four hours after plating, cells were treated with PFFs. Twenty-four hours after treatment with PFFs, cells were washed with PBS and then briefly treated with trypsin to remove residual PFFs bound to the outside membrane of cells or to the dish (for a maximum time of 30 s), incubated again with medium for 5 min (to stop the trypsinization), washed with PBS, and finally, fresh medium was added. Immediately after, cells were treated with fasudil. Regardless of the experimental group, cells were kept for a total of 144 h in an incubator at 37 °C and 5 % CO_2. For RT-QuiC amplification and WB, protein was extracted by cell homogenization with RIPA buffer with PMSF and protease inhibitors.

To study the effect of fasudil on the internalization of α-synuclein by microglia, we carried out a direct cell co-culture experiment to observe potential changes in phagocytosis. For this purpose, we cultured approximately 200,000 HMC3 microglial and N27 neuronal cells in 6-well plates. Once the cells reached a confluence level of 70 %, we proceeded to transfect the N27 cells with α-synuclein fused to EGFP. Simultaneously, we fed HCM3 cells with fresh medium and treated them with 20 μM fasudil. Thirty minutes after fasudil treatment, HCM3 cells were treated with 100 nM AngII. Twenty-four hours later, cells were treated again following the same procedure stated above. Twenty-four hours after the last treatment, HCM3 cells were collected and added to transfected N27 cells. Seventy-two hours later, co-cultured cells were collected for immunocytochemistry and subsequent analysis using flow cytometry.

SiRNA transfection and treatments

For SiRNA transfection, N27 and HMC3 cells transfected with SynT and V5-SPH-1 were left to grow for 24 h or until reaching 80 % confluence. After this, N27 cells were transfected with ROCK2 rat siRNA (MCE, HY-RS12119) and HMC3 cells were transfected with ROCK2 human SiRNA (MC3, HY-RS12117). Transfection was performed by mixing 7 μl of a 20 μM SiRNA stock solution with 2 μl of TurboFect (Thermo Scientific, R0531) and 93 μl of serum-free DMEM medium. Cells were treated with 100 nM AngII 24 h after transfection. Twenty-four hours after AngII treatment, cells were processed for the corresponding experiment.

Immunofluorescence of cell cultures for inclusion quantification

Cells transfected with SynT and V5-SPH-1 were washed with DPBS and fixed with 4 % PFA for 20 min. Following fixation, a blocking and permeabilization step was performed with 1 % BSA, 2 % normal donkey serum (NDS, Sigma), and 1.5 % Triton X-100 in DPBS for 1 h at room temperature. Subsequently, cells were incubated overnight at 4 °C with an anti-α-synuclein antibody MJFR1 (1:1500; Abcam, Rabbit, ab138501) in DPBS with 1 % BSA and 2 % NDS. The cultures were rinsed with DPBS and then incubated for 2 h with the fluorescent secondary antibody Alexa Fluor 488-conjugated donkey anti-rabbit IgG (1:200; Molecular probes). Finally, cultures were incubated for 10 min with the DNA-binding dye Hoechst 33342 (1:8000 in DPBS) and washed three times with DPBS. Preparations were kept at 4 °C until analysis.

Mouse treatments

In the present study, C57BL/6J male mice (8 weeks old at the beginning of the treatment) were used. Mice were divided into three groups. The first group (n = 8) was treated with MPTP (Sigma M0896) alone intraperitoneally for 5 days at a daily dose of 30 mg/kg. A second group (n = 6) was injected with the ROCK inhibitor Y27632 (Sigma, 5 mg/kg/day, intraperitoneally) 30 min before MPTP treatment. A third group (n = 6) was treated with saline for 5 days and used as control group.

Immunohistochemistry of mouse brains

Animals were anesthetized and killed with an overdose of ketamine/xylazine, and perfused, firstly with 0.9 % saline, and then with cold 4 % paraformaldehyde in 0.1 M phosphate buffer, pH 7.4. Brains were removed, washed, and cryoprotected in 0.1 M phosphate buffer containing 20 % sucrose, and cut into 30 μm-thick sections on a freezing microtome. Sections were processed with primary antibodies against α-synuclein MJFR1 (1:500). Additionally, sections were incubated in a 0.1 % solution of thioflavin S (ThS) for 1 h at room temperature, washed three times with 20 mM KPBS, and incubated for 1 h at room temperature with 5 % BSA, 5 % normal serum and 0.3 % Triton X10 in 20 mM KPBS for blocking and permeabilization. After blocking and permeabilization, sections were incubated overnight at 4 °C with the primary antibody. The next day, sections were washed three times with 20 mM KPBS and incubated for 2 h at room temperature with the secondary antibody: Alexa fluor 647 (1:100; Invitrogen by Thermo Fisher, A-31573). Finally, sections were incubated for 10 min at room temperature with a KPBS solution containing 3×10^{-5} M Hoechst 33342 and mounted on gelatin-coated slides using Immumount (Thermo-Shandon, 10622689) as a mounting medium.

Microscopy quantification

For inclusion quantification and size analysis, pictures were taken on a Leica DMI6000B fluorescence microscope equipped with a DFC360FX-31202708 camera at 40 x with a HC PL Fluotar L 40x/0.60 dry objective (reference 11506201) with 460, 527 and 630 nm filters simultaneously. At least 18 (usually 30) pictures were taken for each treatment and experiment. For quantification of α-synuclein inclusions in cell cultures, transfected cells were classified based on the presence or absence of inclusions, and the data were expressed as a percentage of cells with inclusions. The size of α-synuclein inclusions in cell cultures was analyzed with ImageJ's software (https://imagej.nih.gov/ij/). For each image, greyscale 8-bit versions were created, and a threshold of the image was performed and adjusted. Pictures in which the resulting threshold included nuclei or other artifacts were excluded. The resulting image was used to analyze the particle size directly with the analyze particles plug-in.

Mouse brains immunofluorescence was visualized, and pictures taken on a Leica DM4B microscope with a HC PL fluotar 40x objective and a Leica-K5-14401204 camera with 460, 527, 630 and 700 nm filters simultaneously. Quantification of α-synuclein immunorreactivity and binding to ThS was estimated by measurement of particle area via Leica Application Suite X (LAS X, Leica) and ImageJ. The images taken were subjected to a de-blurring process via Thunder Imaging in LAS X. The color threshold of the image was adjusted in ImageJ and the resulting image was used to analyze the particle size directly with the analyze particles plug-in. The area value obtained was expressed as a percentage over the total picture area.

Preparation of pre-formed fibrils

Pre-formed fibrils (PFFs) were prepared based on previously published methods [37–39]. In brief, recombinant α-synuclein (abcam, ab51189) was diluted in PBS up to a concentration of 30 μM and shaken at 750 rpm for 8 days. Formation of PFFs was measured by thioflavin T (ThT) fluorescence emission and by sedimentation assay as follows: for ThT fluorescence emission, samples taken before shaking, at 4 days and after 8 days were diluted in 100 μL PBS up to a concentration of 7 μM. ThT was added to the dilutions to a final concentration of 10 μM and the resulting mix was loaded into black 96-well plates (COSTAR, Corning Incorporated), and fluorescence emission was measured in a plate reader

(Infinite M200 fluorescence plate reader, TECAN) at a wavelength of 480 nm. Samples before shaking, at 4 days and after 8 days were diluted 1:10 in PBS and centrifuged at 10000 g for 30 min and room temperature. Supernatants were collected and pellets were resuspended in 60 μL of PBS. Twelve μL of Laemmli buffer were added to both supernatants and resuspended pellets. Everything was loaded into a 12 % acrylamide gel with a 15-well comb, and SDS-page was performed. After electrophoresis, the acrylamide gels were Coomasie stained and de-stained, and pictures were taken. After checking their formation, PFFs were frozen and kept at −80 °C. Immediately before RT-QuiC, PFFs were thawed and sonicated for 1 min at 30 % intensity with 1-s on, 1-s off pulses.

RT-QuiC

RT-QuiC analyses were performed based on a method previously described [28]. In brief, reactions were performed in black 96-well plates (COSTAR, Corning Incorporated) in which 100 μL of the reaction mixtures were loaded. The final concentrations for each component of the reaction mix were the following: 150 mM NaCl, 1 mM EDTA, 20 μM ThT, 70 μM SDS, 70 μM monomeric α-synuclein and 0.7 μM of PFFs in PBS buffer. Fasudil was added at 20 μM. Some reactions were performed with 40 μM fasudil, added in two times, just before starting the reaction and 20 h after the reaction started. Plates were covered with sealing tape (Axygen UC-500, Corning) and incubated at 41 °C in a plate reader (Infinite M200, TECAN) with intermittent shaking cycles, consisting of 1 min orbital shaking at 432 rpm followed by 2 min incubation and 1 min pause to measure the ThT fluorescence intensity at 480 nm. Two replicates of each sample were measured for 750 amplification cycles (approximately 50 h).

For analyses on cell homogenates, RT-QuiC analyses were performed as described above, with the following changes: in the reaction mix, instead of recombinant PFFs, 2 μg of protein from cell lysates were added. Furthermore, amplification cycles consisted of 1 min orbital shaking at 432 rpm followed by 2 min incubation and a 3-min pause to measure the ThT fluorescence intensity at 480 nm. Two replicates of each sample were measured for 1000 amplification cycles (approximately 100 h).

^{1}H NMR

Proton nuclear magnetic resonance (^{1}H NMR) was performed on a Bruker DRX-500 (Bruker, Germany) magnetic resonance system. Deuterated water (D_2O) used for the solutions had 99.9 % purity (Sigma-Aldrich, St Louis, MO, USA).

WB analyses

Cellular protein levels of α-synuclein, and β-actin were analyzed by WB. The protein was extracted by cell homogenization with RIPA buffer with PMSF and protease and phosphatase inhibitors. Protein extracts were sonicated for 3 s at 10 % amplitude and 25 °C temperature. After that, the total protein concentration was calculated by the Pierce BCA protein assay. Equal amounts of protein were separated by electrophoresis in 12 % bis-tris polyacrylamide gel and transferred to nitrocellulose membranes. The membranes were incubated with primary antibodies against α-synuclein (Ab80627, Abcam; mouse; 1:2000), phosphorylated α-synuclein S129 (Ab59264, Abcam; rabbit 1:2000) and β-actin (A2228, Sigma; 1:10000), overnight at 4 °C. The following day, samples were incubated for 2 h at room temperature with the following fluorescent secondary antibodies: IRDye 680RD (LI-COR; 1:20000) and IRDye 800CW (LI-COR; 1:20000). Immunofluorescence was visualized with a fluorescence detection system (Molecular Imager ChemiDoc MP imaging System, BioRad). Red color was assigned to IRDye 680RD and green to IRDye 800CW. Protein expression was measured by densitometric analysis of each corresponding band using ImageJ's software and expressed relative to the β-actin band value. Phosphorylation levels were measured by calculating the direct relation between phosphorylated and total protein levels for α-synuclein, based on the intensity of the fluorescent dyes. The data were normalized with the control groups (100 %) corresponding to each study group to compare the possible variabilities between both groups.

Autophagy was assessed by WB analysis as follows: Equal amounts of protein were separated by electrophoresis in 15 % bis-tris polyacrylamide gel and transferred to pre-activated PVDF membranes. The membranes were incubated with primary antibodies against LC3b-I/LC3b-II (#12741, Cell signaling; rabbit 1:500) overnight at 4 °C and against β-actin (A2228, Sigma; mouse 1:10000) for 1 h at room temperature. After the incubation with the primary antibodies, samples were incubated for two additional hours at room temperature with the following fluorescent secondary antibodies: IRDye 680RD (LI-COR; 1:20000) and IRDye 800CW (LI-COR; 1:20000). Immunofluorescence was visualized with a fluorescence detection system (Molecular Imager ChemiDoc MP imaging System, BioRad). Red color was assigned to IRDye 680RD and green to IRDye 800CW. LC3b-II and LC3b-I expression levels were determined and normalized to the β-actin band value. Results were expressed as the ratio between LC3b-II and LC3b-I.

Flow cytometry

Initially, 2.5 ml of trypsin were added per well to lift the cells and it was immediately neutralized with FBSi medium. The cell suspension was centrifuged, the supernatant discarded, and the pellet was washed three times with phosphate buffered saline (PBS) and finally resuspended in PBS + 5 % FBSi and kept in ice until analysis. 10000 events were counted for each experiment in a BD Accuri C6 Plus Personal Flow Cytometer. A first gating was performed to separate debris from actual cells based on the FSC and SSC parameters (Fig.S1). A second gating was performed to identify positive cells (above 100000 RFU for green) and negative cells (below a fluorescence level of 100000 RFU for green). Samples were analyzed using BD CSampler plus software (Fig.S2).

To identify microglia while analyzing α-synuclein incorporation by these cell types we performed immunocytochemistry before flow cytometry. To carry out the immunocytochemistry, the primary antibody used was ionized calcium-binding adapter molecule 1 (IBA1 019–19741; 1:500; Abcam, FUJIFILM Wako Pure Chemical Corporation) as a marker of microglia. The corresponding secondary antibody used was Alexa fluor 647 conjugated-donkey anti rabbit (1:100; Invitrogen by Thermo Fisher, A-31573). Fluorescence-activated flow cytometry was performed using a Becton Dickinson (BD) FACSCaliburTM flow cytometer (10000 events analyzed per experiment, filters at 530 nm for EGFP and 670 nm for Alexa fluor). A first gating was performed to separate debris from actual cells based on the FSC and SSC parameters (Fig.S3). A second gating was performed to identify positive cells. Cells with values above 100 RFU for 670 nm and approximately 75 RFU for 530 nm were considered positive (Fig.S3). Samples were analyzed using FlowJo 10.8 software.

For autophagy measurements a red fluorescent autophagy assay kit (AB270790, Abcam) was used following the manufacturer's instructions. HMC3 cells were collected in tripsine, washed with PBS, and marked with the kit's fluorescent probe. Cells were incubated at 37 °C for 30 min, centrifuged at 200 g and washed again 3x with PBS. Fluorescence measurements were performed using a Beckman Coulter Cytoflex cytometer (10000 events analyzed per experiment, filters at 610 nm for red and 525 nm for EGFP). Cells above a fluorescence threshold, established for 610 nm (Fig.S4), were considered positive for autophagy.

NADPH-oxidase activity

N27 and HEK293 cells were collected in krebs-hepes buffer, and homogenized. Protein concentration of the resultant cell suspension was assayed using the Pierce BCA Protein Assay Kit (Thermo Fisher Scientific, Inc., Waltham, MA, USA). Nox activity was measured in 30 μg of extracted proteins in the presence of NADPH (10^{-4} mol/L; Sigma) and lucigenin (5×10^{-6} mol/L; Sigma). Measurements were performed with

an Infinite M200 Pro multiwell plate reader (Tecan, Switzerland). No enzymatic activity was detected in the absence of NADPH.

Rho kinase activity

ROCK activity was measured with a commercially available ROCK Activity Assay kit (CellBiolabs, Inc, San Diego, CA, USA) according to the manufacturer's instructions. This assay is an enzyme immunoassay developed for the detection of the specific phosphorylation of myosin phosphatase target subunit 1 at Thr696 by ROCK. Cells were collected in lysis buffer (50 mM Tris–HCl pH 7.5, 150 mM NaCl, 1 mM beta-glycerolphosphate, 1 mM EDTA, 1 mM EGTA, 1 mM sodium orthovanadate, 1 % Triton X-100) containing protease inhibitor cocktail (P8340, Sigma). The protein concentration of extracts was assayed using the Pierce BCA Protein Assay Kit (Thermo Fisher Scientific, Inc., Waltham, MA, USA) and equal amounts of protein (20 µg per well) were used; each sample was assayed in duplicate. Measurements of phosphorylation activity were performed in an Infinite M200 Pro multiwell plate reader (TECAN) at a wavelength of 450 nm.

Intracellular calcium measurements

To determine changes in intracellular Ca^{2+}, treated and control cells were incubated in 5 µM Fluo-4 AM (Thermo Fisher Scientific) at 37 °C for 60 min and subsequently washed with calcium-free buffer. Live cell fluorescence was analyzed using a widefield microscope (Leica DMI6000B) (488 nm excitation, 520 nm emission). Intracellular Ca2+ changes were measured on individual cells, with each cell defined as one region of interest (ROI) in ImageJ. Changes in fluorescence intensity in each ROI were measured as normalized relative fluorescence (ΔF) relative to basal fluorescence (recording period prior to AngII addition).

Statistical analysis

All statistical analyses were conducted using SigmaPlot 11.0 (Systat Software, Inc., CA, USA). Data normality was evaluated using the Kolmogorov–Smirnov test, while homoscedasticity was assessed using Levene's test. Parametric tests were applied to datasets that satisfied the assumptions of normality and equal variances. Specifically, a Student's *t*-test was used to compare two independent groups, whereas one-way ANOVA followed by the most appropriate post hoc test was employed for comparisons involving more than two groups. For datasets that violated the assumption of normality, non-parametric tests were utilized. The Mann–Whitney *U* test was performed for comparisons between two groups, and the Kruskal–Wallis test was applied for comparisons across multiple groups. Post hoc pairwise analyses for non-parametric data were carried out using the most appropriate test. Differences were considered statistically significant at $p \leq 0.05$. All graphs were carried out with GraphPad Prism 8. Data were obtained from at least 6 independent experiments and were expressed as means ± standard error of the mean (SEM). For the PFFs preparation, data from 3 independent measurements were analyzed and expressed as means ± standard deviation of the mean. For PFF-seeding RT-QuIC experiments, data from 6 independent biological replicates were analyzed as means ± SEM.

Results

Fasudil inhibits AngII-mediated increase in α-synuclein aggregation

Initially, we decided to study the effects that fasudil may have in the AngII-induced increase in the number and nature of the inclusions in the different cell types. We analyzed the number of cells with inclusions and the average inclusion size using the SynT/Sph1 model (Fig. 2). In the N27 dopaminergic neuronal cells, treatment with AngII significantly

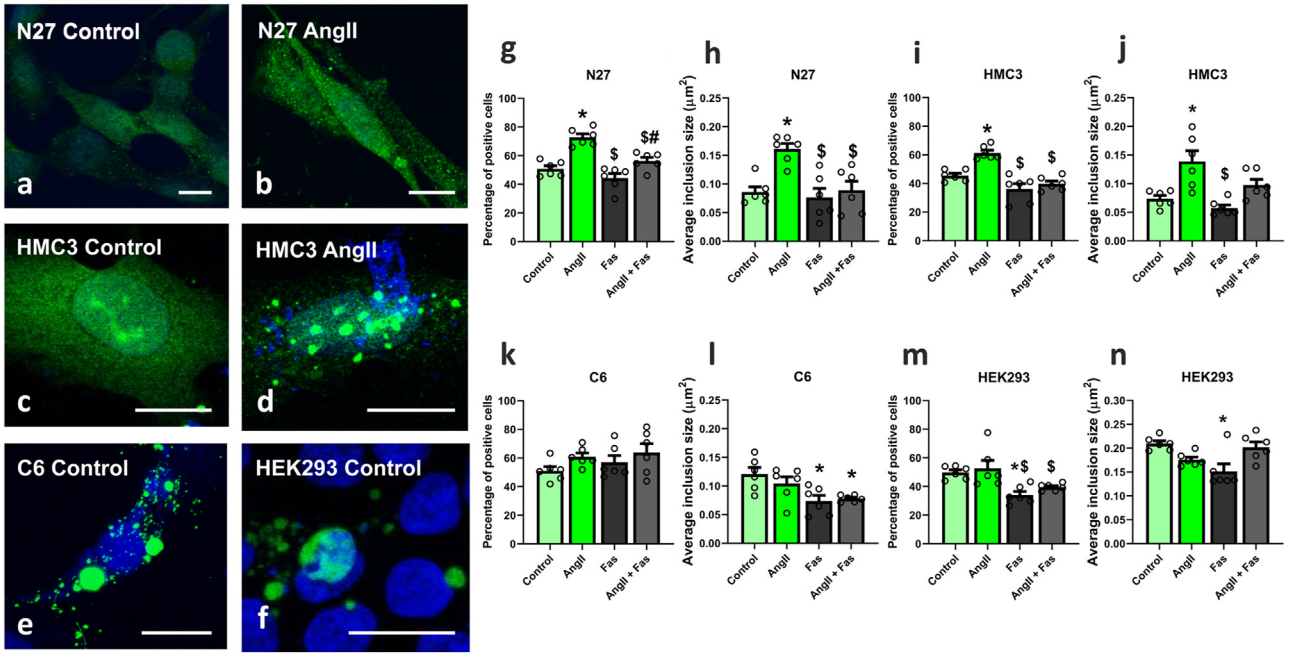

Fig. 2. Fasudil decreases AngII-mediated increase in cells showing inclusions and in average inclusion size in N27 and HMC3 cells. Cells were transfected as indicated in Fig. 1. **(a–f)**: Representative confocal microphotographs of the cells analyzed. **(g–h)**: Treatment with AngII in N27 cells leads to a significant increase in the percentage of cells showing inclusions and in the average inclusion size that are reverted with treatment with fasudil. **(i–j)**: Treatment with AngII in HMC3 cells leads to a significant increase in the percentage of cells showing inclusions and in the average inclusion size that are blocked after treatment with fasudil. Treatment with fasudil alone leads to a significant decrease in inclusion size in relation to controls. **(k–n)**: Treatment with AngII in C6 and HEK293 cells did not lead to significant changes in the percentage of positive cells, nor in the average inclusion size. Fasudil alone leads to a significant decrease in the inclusion size, and in the case of HEK293 in percentage of cells showing inclusions. Average inclusion size decreases after treatment with AngII and fasudil in C6 cells. n = 6 independent experiments, at least 30 pictures were analyzed for each treatment and experiment. Scale bars 12 µm. AngII: Angiotensin II. Fas: Fasudil. $^{*}P < 0.05$ relative to control. $^{\$}P < 0.05$ relative to AngII. $^{\#}P < 0.05$ relative to Fasudil. One-way ANOVA and Tukey's multiple comparison test. Error bars represent SEM.

increased the percentage of cells positive for inclusions, which was blocked by treatment with the ROCK inhibitor fasudil (Fig. 2g). Similar results were observed in the average inclusion size (Fig. 2h). This suggests that AngII induces the formation of a higher number of bigger α-synuclein aggregates that is blocked after treatment with the ROCK inhibitor fasudil.

We observed similar results in HMC3 microglial cells. After treatment with AngII, a higher number of cells showed inclusions and a higher average inclusion size was observed (Fig. 2i and j), pointing to the formation of a higher number of bigger α-synuclein aggregates, which was inhibited by fasudil.

In the C6 astrocytic cells, the different treatments did not lead to any significant change in the number of cells with inclusions (Fig. 2k). However, we observed a significant decrease in inclusion size after treatment with fasudil or fasudil and AngII (Fig. 2l).

In HEK293 cells, we did not observe any significant changes after treatment with AngII (Fig. 2m and n). It has been shown that HEK293 cells lack AT1 receptors [27,40], and these results could be expected. However, treatment with fasudil led to a significantly lower number of cells with inclusions and inclusion size, pointing to fasudil effects on α-synuclein aggregation independent from its effects on the AngII/AT1 pathway. This suggests that fasudil may act also through additional pathways or mechanisms, which were addressed in the following experiments.

Treatments with AngII or fasudil do not change α-synuclein protein expression or phosphorylation

To assess whether the changes observed in the number of cells with inclusions or size of the inclusions after the different treatments are due to changes in protein expression instead of a higher tendency to form aggregates, we performed SDS-PAGE western blots of the cells analyzed by microscopy. No significant changes in protein expression were observed after the different treatments (Fig. 3a, b, c, d). Furthermore, as α-synuclein phosphorylation may change the ability of α-synuclein to form aggregates or the internalization of the protein [41], we measured, by fluorescent Western blot, the phosphorylation levels of α-synuclein at Ser129 after the different treatments. We did not observe any change in α-synuclein phosphorylation levels due to the different treatments (Fig. 3e, f, g, h). These results imply that the changes in the percentage of cells with inclusions and average α-synuclein inclusion size are not due to changes in protein expression, nor due to changes in α-synuclein phosphorylation levels at Ser129.

α-synuclein aggregation is not inhibited by direct interaction between fasudil and α-synuclein

It has been proposed that fasudil can directly bind to α-synuclein blocking the addition of new monomers, which may lead to a blockade

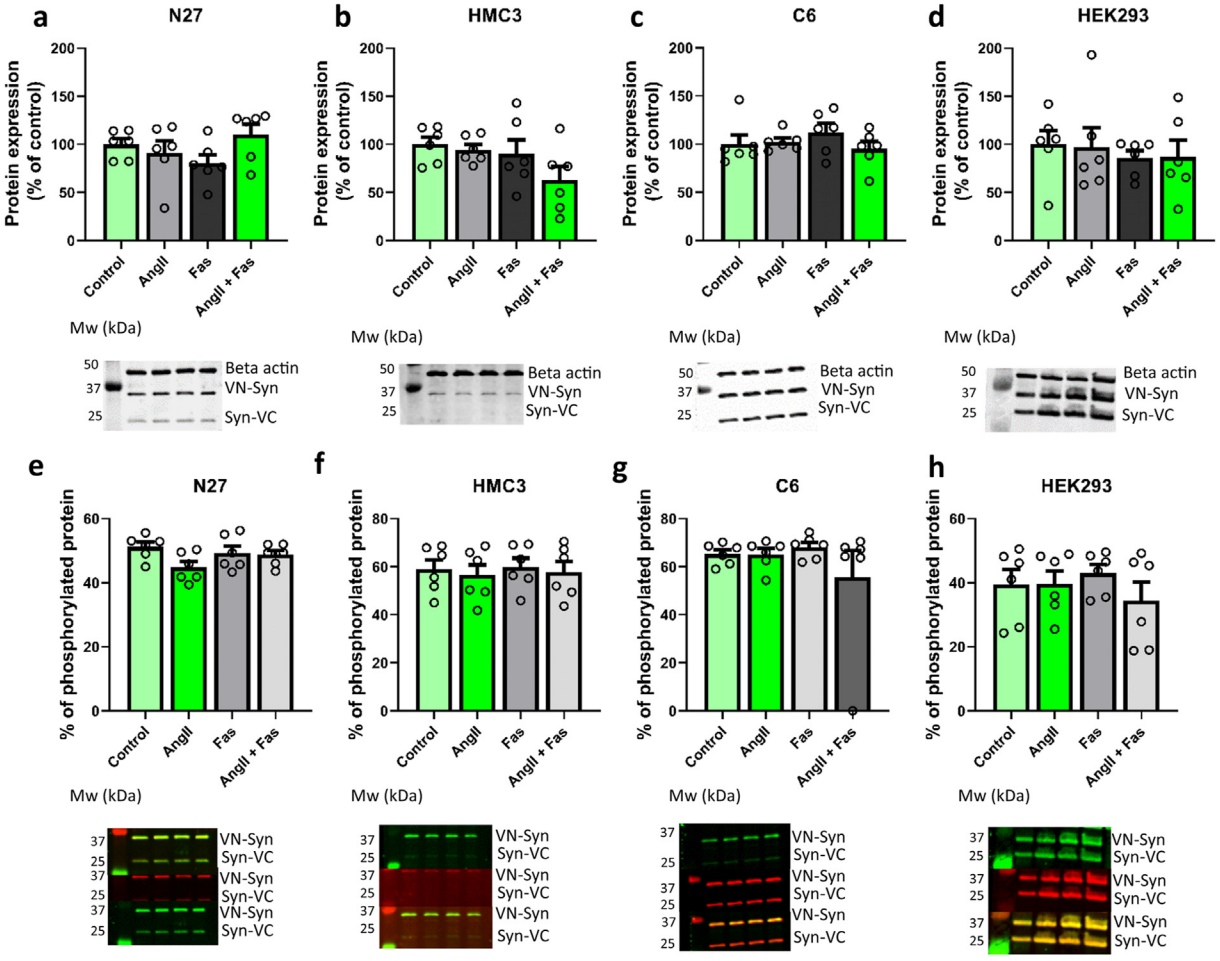

Fig. 3. Western blot analyses show no significant changes in α-synuclein expression nor in α-synuclein phosphorylation. Cells were transfected with VNSyn/SynVC to measure α-synuclein expression. **(a–d)**: Western blot analyses of N27, HMC3, C6 and HEK293 cells showed no significant changes due to the different treatments. **(e–h)**: Western blot analyses of N27, HMC3, C6 and HEK293 cells showed no differences in α-synuclein phosphorylation levels due to the different treatments. Green = Phosphorylated α-synuclein. Red = Not phosphorylated α-synuclein. n = 6 independent measurements. AngII: Angiotensin II. Fas: Fasudil. One-way ANOVA (a–f), and Kruskal-Wallis one way analysis on ranks (g–h). Error bars represent SEM.

of the formation of high molecular weight species [18,19]. To assess the direct interaction between α-synuclein and fasudil, we performed a RT-QuiC assay. Before performing the assay, we checked the preparation of the PFFs that we used as seeds for the assay. Eight days after starting the preparation process, the results in the sedimentation assay and ThT staining were significantly different from the results obtained for the recombinant protein before starting the preparation of PFFs (Fig. 4a, b, c, d). The results showed that the PFFs were ready 8 days after starting their preparation. Our RT-QuiC results showed an increase in lag time, although no significant differences in the area under the curve, endpoint ThT fluorescence, and the aggregation constant due to fasudil treatment in seeded reactions (Fig. 4e, f, g, h, i).

RT-QuiC amplification does not degrade fasudil

To determine whether the lack of aggregation inhibition observed by RT-QuIC could be due to the degradation of fasudil or fibrils during the RT-QuIC process, we performed three different experiments. First, we analyzed whether the addition of fasudil to already formed fibrils may lead to their degradation. Our results showed no decrease in ThT fluorescence, which indicates that the fibrils suffer no degradation (Fig. 4j). The second experiment was the addition of fasudil 20 h after starting the RT-QuIC process, approximately the moment in which aggregation would start. If fasudil is degraded, new fasudil will inhibit aggregation. However, our results showed that when we added 20 μM of new fasudil, the fluorescence curves became steeper relative to the control curves

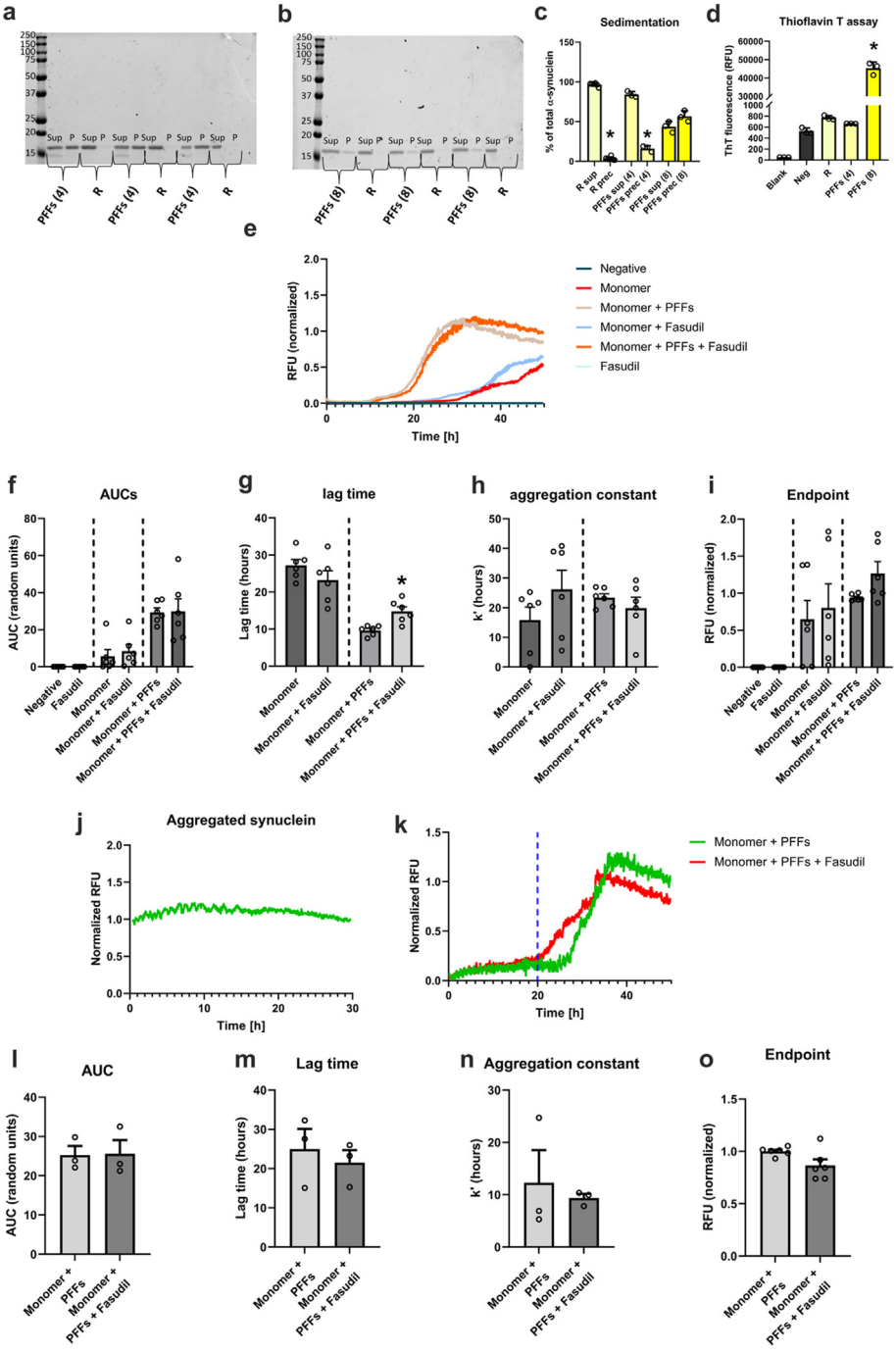

Fig. 4. RT-QuiC analyses. **(a–b)**: Coomassie staining of acrylamide gels shows the presence of PFFs 8 days after starting the preparation process. **(c)**: Quantification of Coomassie-stained gels showed a higher significant quantity of protein in supernatants before starting the PFFs preparation process and after 4 days. *P < 0.05 relative to the previous column. n = 3. Mann-Whitney *U* test and *t*-test. Error bars represent SD. **(d)**: ThT assay of PFFs shows a significant increase in ThT fluorescence in samples collected at 8 days after starting the preparation process. R: Recombinant monomeric protein; sup: supernatant; prec: precipitate; PFFs: Pre-formed fibrils (4): Sample after four days of shaking; PFFs (8): Sample after eight days of shaking. *P < 0.05 relative to R. n = 3 independent measurements. One-way ANOVA and Tukey's multiple comparison test. Error bars represent SD. **(e)**: RT-QuiC graph of the monomeric α-synuclein amplification in the presence and absence of 20 μM fasudil. **(f–i)**: Treatment with fasudil does not lead to significant changes in AUC, lag time, aggregation constant, nor in normalized RFU values at the end of the assay for unseeded RT-QuiC reactions. Treatment with fasudil significantly increases the lag time of the aggregation process in seeded RT-QuiC reactions. **(j)**: Treatment with fasudil does not affect already aggregated α-synuclein. **(k)**: RT-QuiC graph of monomeric α-synuclein amplification in the presence and absence of 40 μM fasudil, added at the onset of reaction and after 20 h (dotted line). **(l–o)**: A second fasudil treatment 20 h after the onset of the process does not lead to significant changes in AUC, lag times, aggregation constant, nor in normalized RFU values at the end of the assay for seeded RT-QuiC reactions. n = 3–6 independent amplifications. *P < 0.05 relative to Monomer + PFFs. Error bars represent SEM. Mann-Whitney *U* test (f, i) or two-tailed unpaired Student's t-test (g-h, l-o).

(Fig. 4k). This effect is the consequence of a faster aggregation rate. No significant differences in the area under the curve, lag time, aggregation constant nor in endpoint ThT fluorescence, due to fasudil treatment were observed (Fig. 4l, m, n, o) The main binding sites of fasudil on α-Syn are tyrosines Y125, Y133 and Y136 at the *C*-terminal region. However, it has been proposed that an excess of fasudil may bind to Y39 (in the amphipathic region) in addition to the aforementioned tyrosines, thus changing the amphipathic properties of α-synuclein which lead to higher aggregation rates [18,42]. Finally, in a third experiment, we checked the stability of fasudil during the RT-QuIC process. To check this, we performed the RT-QuIC process in the absence of α-synuclein and ThT in one of the wells. Aliquots of this sample were collected before and after the RT-QuIC process and ^{1}H NMR (proton nuclear magnetic resonance) was performed to compare them. If the process affected the stability of fasudil, we would have observed changes in chemical shifts. Our ^{1}H NMR results were the following: ^{1}H NMR (500 MHz, D_2O) δ 9.06 (d, J = 0.9 Hz, 1H), 8.38 (d, J = 6.2 Hz, 1H), 8.17–8.07 (m, 3H), 7.61 (t, J = 7.8 Hz, 1H), 3.65 (m, 2H), 3.45 (t, J = 6.2 Hz, 2H), 3.36–3.29 (m, 4H), 2.07 (p, J = 6.0 Hz, 2H) for the sample before RT-QuIC and ^{1}H NMR (500 MHz, D_2O) δ 9.07 (d, J = 0.9 Hz, 1H), 8.39 (d, J = 6.2 Hz, 1H), 8.19–8.08 (m, 3H), 7.62 (t, J = 7.8 Hz, 1H), 3.65 (m, 2H), 3.45 (t, J = 6.2 Hz, 2H), 3.36–3.28 (m, 4H), 2.07 (p, J = 5.9 Hz, 2H) for the sample after RT-QuIC. Solvent signal at δ 4.70. The results showed no significant changes in chemical shift, proving that fasudil did not suffer any degradation during the RT-QuIC process (Fig.S5).

Fasudil inhibits PFF-induced seeding activity of α-synuclein in N27 cells

To study the possibility that fasudil may have additional mechanisms to cope with PFF-induced seeding in cells than direct molecule-molecule interaction, we treated N27 cells with PFFs to induce α-synuclein aggregation. Twenty-four hours later, cells were washed and then treated with fasudil. Cell homogenates were added to RT-QuIC reaction mixes and amplifications were performed. Our results showed a significant decrease in lag time and significant increases in AUC, endpoint ThT fluorescence, and aggregation constant in PFF-seeded cells in comparison with control cells and cells treated with fasudil (Fig. 5). These results show that, *on cell homogenates*, fasudil has a clear effect blocking α-synuclein aggregation. This further supports that direct molecule-molecule interaction is not the main mechanism by which fasudil inhibits α-synuclein aggregation.

ROCK inhibition mediates the effects of fasudil on α-synuclein aggregation

The above-described data suggest that the effects of fasudil on α-synuclein aggregation are via ROCK inhibition rather than through specific effects of the fasudil molecule. To confirm this, we studied the effects of fasudil and a different ROCK inhibitor (Y27632) *in vitro* and *in vivo*.

To confirm that the observed effects were related to fasudil-induced decrease in ROCK activity, we measured ROCK activity in N27 cells. Both AngII/AT1 activation and α-synuclein overexpression and accumulation induced a significant increase in ROCK activity, which was blocked by treatment with fasudil. In addition, the inhibitory effects of fasudil on ROCK activity were reproduced with a second ROCK inhibitor Y27632 (Fig. 6a).

Furthermore, we confirmed that α-synuclein aggregation was also reduced *in vitro* by a second ROCK inhibitor (Y27632). In N27 neuronal cells, the increase in number of cells with inclusions and size of the aggregates induced by AngII/AT1 activation was blocked by treatment with Y27632 (Fig. 6b and c), as observed with fasudil. In addition to this, we performed inhibition of ROCK gene expression with SiRNA in N27 neuronal cells and HMC3 cells. Our results show that ROCK silencing inhibits the increase in number of cells with inclusions and size of the aggregates induced by AngII/AT1 activation, further confirming that fasudil effects on α-synuclein aggregation are via ROCK inhibition (Fig. 6d, e, f, g).

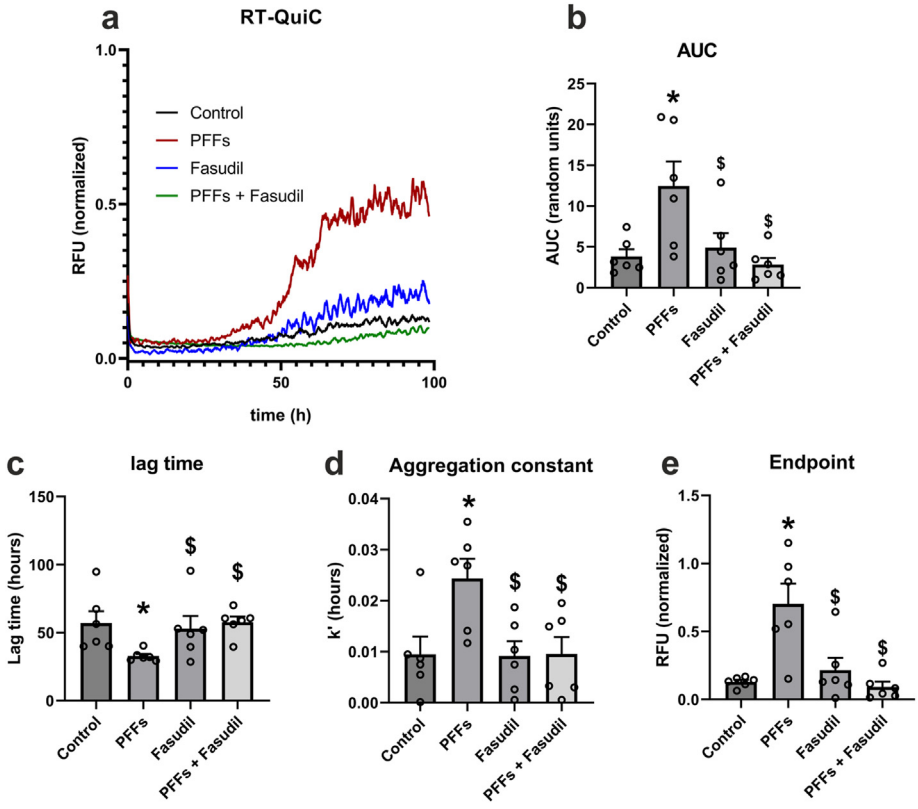

Fig. 5. RT-QuiC analysis of cell homogenates. **(a)**: RT-QuiC graph of the monomeric α-synuclein amplification in the presence and absence of 2 μg of protein from cell lysates fasudil. **(b–e)**: Protein extracts from cells treated with 100 nM of PFFs lead to significant changes in AUC, lag time, aggregation constant and in normalized RFU values at the end of the assay. All changes are reverted by treatment with fasudil. *P < 0.05 relative to control. $^{\$}$P < 0.05 relative to PFFs. ANOVA (d) and ANOVA on ranks (b-c, e) followed by Student-Newman-Keuls method. Error bars represent SEM.

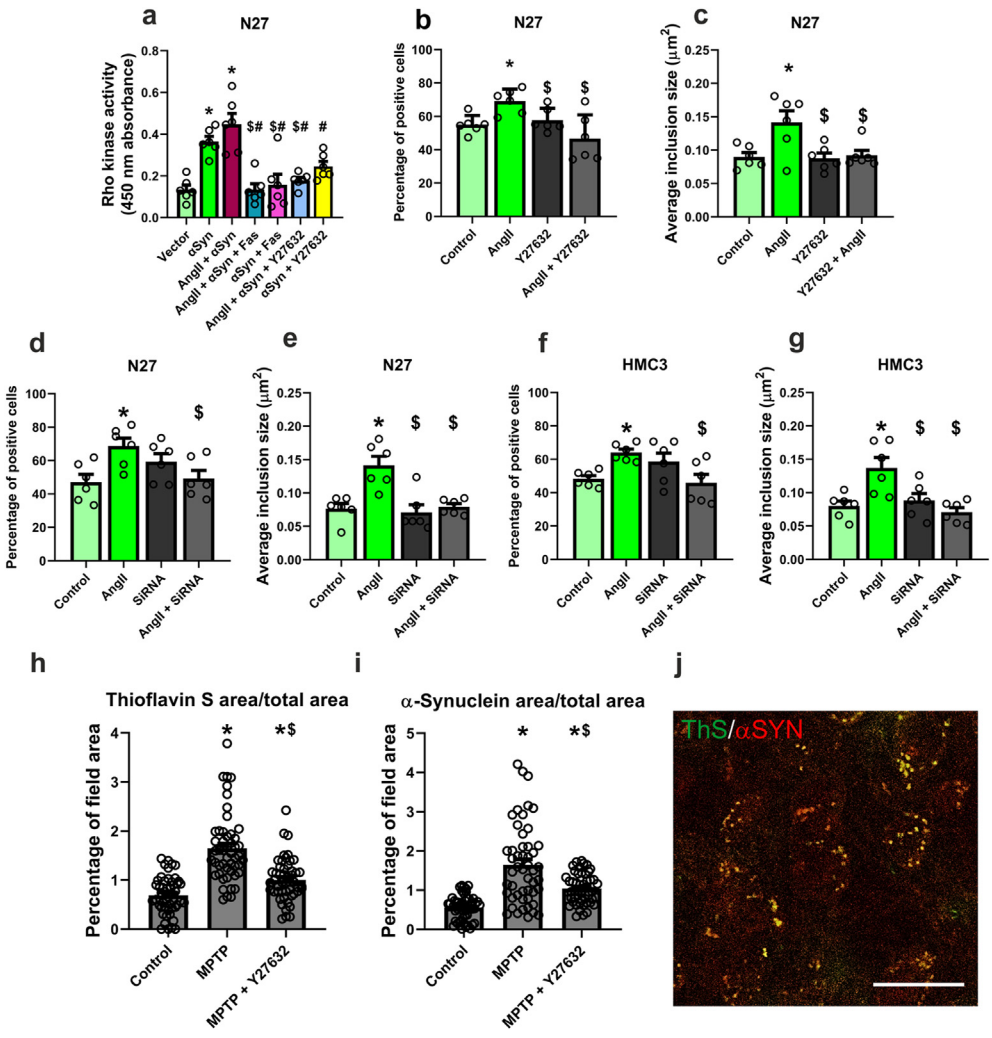

Fig. 6. ROCK inhibition mediates the effects of fasudil on α-synuclein aggregation. **(a)**: Treatment with fasudil or Y27632 blocks the increase in ROCK activity due to AngII stimulation and/or α-synuclein overexpression. n = 6 independent experiments. *P < 0.05 relative to vector. $P < 0.05 relative to αSyn. #P < 0.05 relative to AngII + αSyn. One way ANOVA and Tukey's multiple comparison test. Error bars represent SEM. **(b–c)**: Treatment with AngII in N27 cells leads to a significant increase in the percentage of cells showing inclusions and in the average inclusion size, which are reverted by treatment with a different ROCK inhibitor (Y27632). n = 6 independent experiments. *P < 0.05 relative to control. $P < 0.05 relative to AngII. One way ANOVA followed by Student-Newman-Keuls Method. Error bars represent SEM. **(d–g)**: Inhibition of ROCK expression with SiRNAs blocked the increase in the percentage of cells showing inclusions and in the average inclusion size of AngII-treated N27 and HMC3 cells. N = 6 independent experiments. 18 to 30 pictures were analyzed for each treatment and experiment. *P < 0.05 relative to control. $P < 0.05 relative to AngII. One way ANOVA and Tukey's multiple comparison test (d-e, g); Kruskal-Wallis one way analysis on ranks followed by Student-Newman-Keuls Method (f). Error bars represent SEM. **(h–j)**: Treatment with MPTP induced the formation of inclusions in striatum, as observed in confocal pictures. Treatment with MPTP led to a significant increase in thioflavin S-positive staining and in α-synuclein expression in the striatum, which were inhibited by treatment with the ROCK inhibitor Y27632. n = 50 pictures analyzed. *P < 0.05 relative to control. $P < 0.05 relative to MPTP. Kruskal-Wallis one way analysis on ranks followed by Tukey's multiple comparison test (h) and Student-Newman-Keuls Method (i). Error bars represent SEM. ThS: Thioflavin S (green). αSyn: α-synuclein (red). Scale bar: 20 μm.

We used the MPTP mice model to confirm that the effect of ROCK inhibition on α-synuclein aggregation observed *in vitro* was also produced *in vivo*. As in previous studies from our laboratory and others, MPTP induced a significant increase in α-synuclein aggregation, measured as Thioflavin S (ThS) signal, and in α-synuclein immunoreactivity in the mouse striatum (see for details [23,25]). The combination of α-synuclein immunoreactivity and ThS staining is performed to check the nature of these ThS signals. The identity of these ThS positive signals has been identified by immunoreactivity and Western blot as detailed in our recent study using the same model [23]. In the present study, we observed that the increasing effect on α-synuclein aggregation induced by the MPTP treatment was significantly inhibited by simultaneous treatment of mice with the ROCK inhibitor Y27632 (Fig. 6h, i, j).

Fasudil inhibits α-synuclein endocytosis in microglia

The present results show that the effects of fasudil on α-synuclein aggregation are via ROCK inhibition. Therefore, we analyzed possible ROCK-related mechanisms involved in these effects. As ROCK is one of the proteins regulating membrane changes that may facilitate endocytic processes [43], we studied if the fasudil effects may be at least partially related to alterations in cell endocytosis. We performed direct co-cultures adding untreated, AngII-treated, fasudil-treated or AngII plus fasudil-treated microglial HMC3 cells to N27 dopaminergic neurons expressing α-synuclein-EGFP. We observed a significant increase in α-synuclein-EGFP-positive microglia after treatment with AngII, which was blocked after treatment with fasudil. These results imply that fasudil has an inhibitory effect on the microglial endocytosis, even though fasudil alone did not have a significant effect relative to controls (Fig. 7a and b). This difference may be because AngII exacerbates the activity of the RhoA/ROCK pathway, which is blocked by fasudil.

The transfection process is not affected when fasudil is administered 48 h post-transfection

As shown above, ROCK inhibition may lead to alterations in the incorporation of the α-synuclein DNA plasmids over time, thus leading to lower dimer and oligomer formation and lower fluorescence intensity [44,45]. To prevent the effects of this mechanism from masking possible direct effects of ROCK inhibition on α-synuclein aggregation, we performed the treatments with fasudil 48 h after transfection. Our flow cytometry results showed that treatment with fasudil does not affect

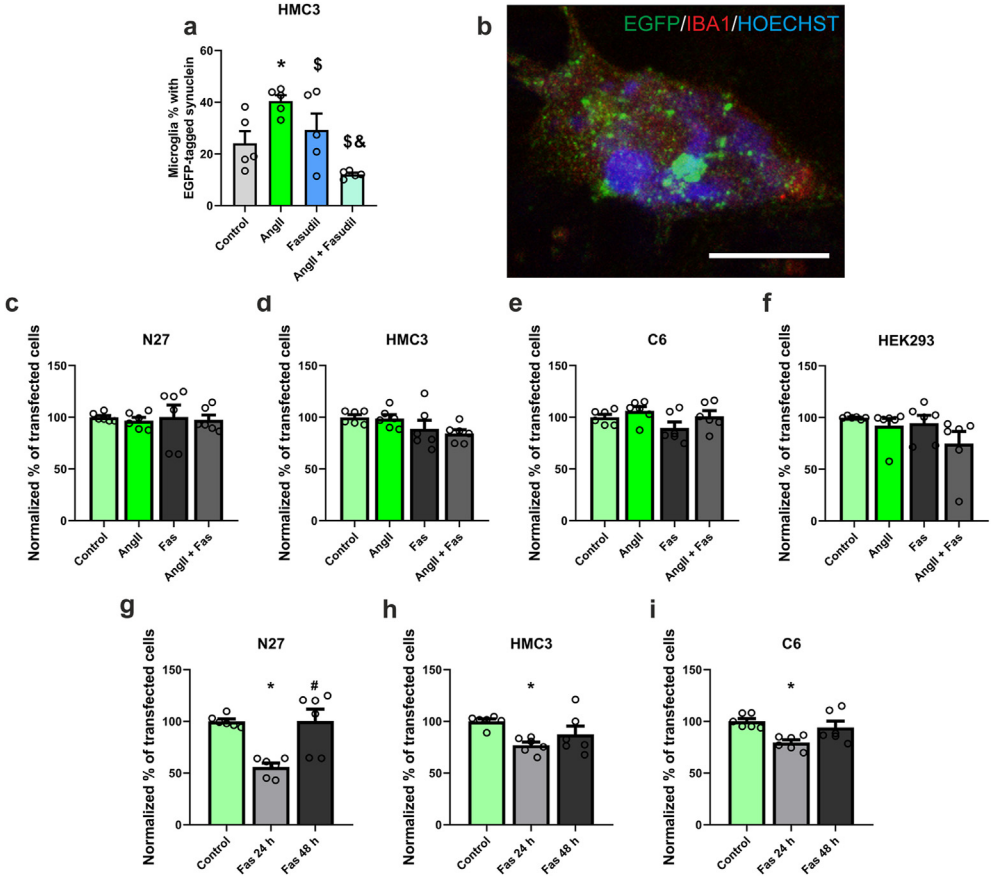

Fig. 7. Effects of fasudil on endocytosis and plasmid internalization. **(a)**: AngII significantly increases the internalization of α-synuclein by microglia, which is blocked after treatment with fasudil. n = 5 independent experiments. *P < 0.05 relative to control. $P < 0.05 relative to AngII. &P < 0.05 relative to Fasudil. One-way ANOVA and Holm-Sidak's test. **(b)**: Representative confocal picture of HMC3 cells (red) that have internalized α-synuclein (green). Scale bar: 12 μm. **(c–f)**: Flow cytometry analyses of the different cell treatments do not show differences in α-synuclein transfection for VNSyn and SynVC after AngII treatment or fasudil treatment 48 h after transfection. One-way ANOVA. Error bars represent SEM. **(g–i)**: Flow cytometry analyses show that fasudil affects transfection if the treatment is performed in less than 24 h after transfection, but not 48 h later. n = 6 independent measurements. AngII: Angiotensin II. Fas: Fasudil. *P < 0.05 relative to control. #P < 0.05 relative to Fas 24 h. One-way ANOVA and Tukey's multiple comparison test. Error bars represent SEM.

plasmid internalization or expression if the treatment is performed 48 h after transfection (Fig. 7c, d, e, f). However, plasmid internalization may be affected if treatments are performed earlier, such as 24 h after transfection (Fig. 7g, h, i). Therefore, this mechanism did not affect the results of the present study.

Fasudil inhibits the increase in NADPH-oxidase activity induced by AngII/AT1 activation and α-synuclein accumulation

NADPH-oxidase-derived oxidative stress has been considered a major factor inducing α-synuclein aggregation into oligomers [46–48], which we have recently confirmed in N27 neuronal cells [23]. As both AngII/AT1 activation [49,50] and α-synuclein accumulation [16] increase NADPH-oxidase activity, we studied if this enhancing effect on NADPH-oxidase activity may be inhibited by fasudil. In N27 cells overexpressing α-synuclein, treatment with AngII increased NADPH oxidase activity, and this was reverted to control values (i.e. cells transfected with empty transfection vectors) after treatment with the ROCK inhibitor fasudil (Fig. 8a and b). In HEK293 cells, we confirmed that overexpression of α-synuclein increased the NADPH oxidase activity. This effect did not change after treatment with AngII because HEK293 cells lack receptors for AngII. However, treatment with fasudil inhibited the increase in NADPH-oxidase activity in HEK293 cells (Fig. 8c and d). In addition, similar effects were induced by a second ROCK inhibitor, Y27632 (Fig. 8a, b, c, d), which further confirms that they are related to ROCK inhibition rather than to specific fasudil properties.

Fasudil inhibits intraneuronal calcium raising

Intraneuronal calcium raising has been related to promotion of α-synuclein aggregation [51,52]. In N27 cells, treatment with fasudil alone led to a significant decrease in calcium levels relative to control untreated cells. At the doses used in the present study, the decrease in calcium levels induced by Y27632 alone did not reach statistical significance. However, both fasudil and Y27632 blocked the increase in intracellular calcium induced by AngII (Fig. 8e and f).

It is known that AngII/AT1 activation promotes intraneuronal calcium raising [53–55]. Our results confirmed that AngII increases intracellular calcium in N27 cells, and that ROCK inhibition blocks the increase in intracellular calcium levels, which promote α-synuclein aggregation.

Fasudil enhances autophagy

Another mechanism by which ROCK inhibition may reduce the accumulation of α-synuclein aggregates is by increasing the autophagic process. In HMC3 cells, we measured autophagy levels by WB. Autophagy is usually assessed by WB with an antibody detecting microtubule-associated protein 1 light chain 3 beta (LC3b). During autophagy, soluble LC3b-I is converted to LC3b-II, which is associated with autophagosomes. The relation between both isoforms is used to measure autophagy [56]. We observed that fasudil increased autophagy levels, which was also observed using a different ROCK inhibitor (Y27632), suggesting that the effect was mediated by the inhibition of ROCK activity (Fig. 8g and h). Furthermore, we confirmed the results by flow cytometry using a commercially available autophagy assay (Fig. 8j and k). To check the validity of both WB and flow cytometry results, cells were treated with the autophagy inhibitor bafilomycin and the autophagy enhancer rapamycin (Fig. 8i and l).

Discussion

The present results show that fasudil inhibits the AngII-induced increase in the number of cells with inclusions and the size of the inclusions in neurons and glial cells suggesting a decrease in α-synuclein

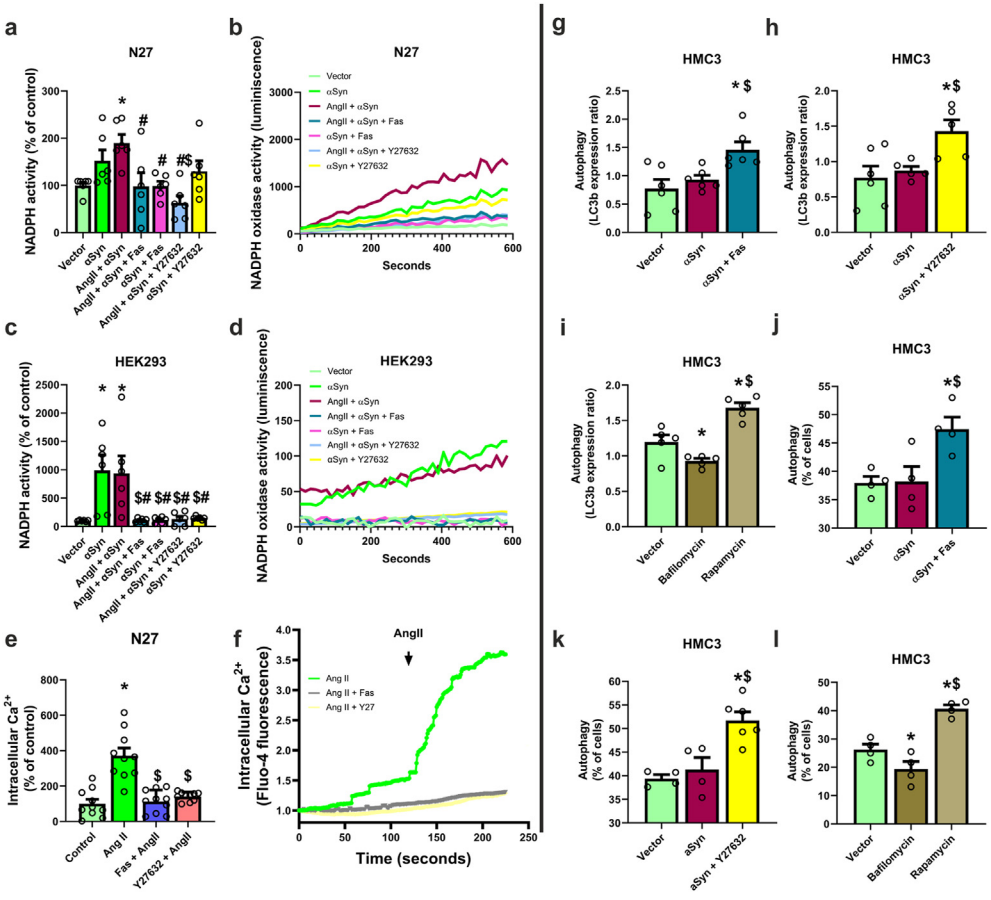

Fig. 8. NADPH-oxidase (Nox) activation increased with α-synuclein overexpression and AngII/AT1 activation in **(a–b)** in N27 cells and **(c–d)** HEK293 cells. Treatment with fasudil or Y27632 blocked this effect. **(e–f)**: Treatment with fasudil or Y27632 blocked calcium release induced by AngII. n = 10 cells measured. **(g-h):** Western blot quantification showing that fasudil and Y27632 increased autophagy in HMC3 cells overexpressing α-synuclein. **(i)**: Treatment with the autophagy inhibitor bafilomycin leads to a significant decrease in autophagy, while treatment with the autophagy inducer rapamycin leads to a significant increase in autophagy in HMC3 cells as measured by Western blot. Representative full blots are shown in Fig.S6. n = 5–6. **(j–k)**: Flow cytometry quantification showing that fasudil and Y27632 increased autophagy in HMC3 cells overexpressing α-synuclein. **(l)**: Treatment with the autophagy inhibitor bafilomycin leads to a significant decrease in autophagy, while treatment with the autophagy inducer rapamycin leads to a significant increase in autophagy in HMC3 cells as measured by flow cytometry. n = 4–6. *P < 0.05 relative to vector (a, c, g-l); relative to control (e). $P < 0.05 relative to α-synuclein (a, c); relative to AngII (e); relative to α-synuclein (g, h, j, k); relative to Bafilomycin (i, l). #P < 0.05 relative to α-synuclein + AngII. Kruskal-Wallis one way analysis on ranks (c, e) followed by Student-Newman-Keuls Method (c) or Tukey's multiple comparison test (e); one-way ANOVA followed by Tukey's multiple comparison test (a, g, h, j, k) or Student-Newman-Keuls Method (i, l). Error bars represent SEM.

aggregation. Furthermore, we also detected a significant decrease in the inclusion size after treatment with fasudil alone (i.e. in the absence of AngII) relative to controls in HEK293 and astrocytes, but not in N27 dopaminergic cells. N27 neuronal cells show a higher number of smaller inclusions [23], so significant changes in the size of aggregates may be more difficult to detect in N27. As previously observed [23], administration of AngII to cultures of C6 astrocytes did not increase the number of cells with inclusion or the inclusion size, possibly because astrocytes are the major source of brain endogenous angiotensin [57,58], and further administration of AngII is not effective. However, administration of fasudil to C6 astrocyte cultures significantly decreased the size of the inclusions. Interestingly, treatment with fasudil was also effective in decreasing the number of cells with inclusions and the inclusion size in HEK293 cells lacking AngII receptors [26,27], which indicates that the effect of fasudil on α-synuclein aggregation is not just related to the inhibition of the AngII effects.

We excluded that the effect of fasudil on α-synuclein aggregation could be an indirect consequence of effects on protein expression or protein phosphorylation, rather than a change in the tendency to form aggregates. In a healthy brain, most α-synuclein is unphosphorylated while aggregated α-synuclein in LB is mostly phosphorylated at Ser129, thus increased expression or phosphorylation of α-synuclein may affect aggregation [41,59]. However, we have observed that the changes produced in the different cells after treatments with AngII or fasudil are not due to significant changes in α-synuclein expression, nor changes in α-synuclein phosphorylation.

It has been previously proposed that fasudil may inhibit α-synuclein aggregation by direct molecule-molecule interaction, independent of its effect on ROCK activity [18,19]. However, our results show that the fasudil-induced decrease in the markers of aggregation in neuronal, glial cells, and HEK293 cells is mostly related to inhibition of ROCK activity. We observed no decrease in α-synuclein aggregation but a delay in seeded RT-QuiC reactions. Initially, we observed the same effects as previous works suggesting direct effects of fasudil, but as we kept the reaction going, the ThT fluorescence levels of the fasudil-treated group reached the same values as the untreated group, indicating that direct molecule-molecule interaction between fasudil and α-synuclein does not lead to a decrease in α-synuclein aggregation. Otherwise, the final ThT fluorescence levels would have been lower in the fasudil-treated group.

However, different experimental conditions, as in the aforementioned studies, might result in varying effects on the final levels of aggregation. To explore this possibility further, we conducted an additional experiment to evaluate whether fasudil degradation during the process or insufficient dosing could explain the observed results (i.e. increased lag time and no decrease in α-synuclein aggregation). A second dose of fasudil was added during amplification. Again, no significant effect of fasudil on the aggregation constant or endpoint ThT fluorescence was detected. Moreover, no significant differences in lag time were observed after the second dose compared to controls. This suggests that a second dose accelerated the aggregation rate compared to a single dose. A possible explanation for this effect on lag time may be that an excess of fasudil may bind to Y39 (in the amphipathic region) in addition to the tyrosines mentioned above, thus changing the amphipathic properties of α-synuclein, which leads to higher aggregation rates [18,42]. These observations, together with the fact that fasudil alone does not affect monomer aggregation in the absence of seeds, further confirms that a direct interaction between fasudil and α-synuclein is not the main

responsible for its final effect on α-synuclein aggregation. Additionally, fasudil treatment *in cellulo* blocked α-synuclein aggregation after treatment with PFFs. PFFs act as aggregation seeds inside the cells, forming α-synuclein aggregates composed of α-synuclein phosphorylated at Ser129 [35]. The aggregates formed inside cells act as aggregation seeds in the RT-QuiC amplification. Our data suggest that the ROCK pathway is involved in the increase in α-synuclein aggregation and that inhibition of ROCK activity by fasudil is the major responsible for the reduction of α-synuclein aggregation. In neurons, ROCK regulates vesicle mobilization, vesicle cycling, and motility in synapses [60–62]. In glial cells, ROCK regulates pro-inflammatory activation, cytokinetic segregation of glial filaments, and migration [60,63,64]. Consistent with this, activation of the RhoA/ROCK pathway leads to increased microglial inflammatory responses, apoptotic processes, and axon degeneration increasing dopaminergic neuron death in PD models [12,13,15]. The present results suggest that ROCK activation also promotes α-synuclein aggregation. Furthermore, we observed that α-synuclein aggregation is increased by factors that upregulate ROCK activity such as AngII/AT1 activation and MPTP treatment [12,13], and it is decreased by ROCK inhibitors, including not only fasudil but also other specific ROCK inhibitors, such as Y27632, and ROCK SiRNA. Interestingly, the present results suggest that α-synuclein aggregation by itself can lead to higher ROCK activity. This, in turn, leads to higher AngII/AT1 activity and higher α-synuclein aggregation levels [17,65]. Interruption of these mutual interactions using fasudil or Y27632 may lead to the lower α-synuclein aggregation levels observed in the present study.

We studied several potential mechanisms that could link ROCK activation and α-synuclein aggregation. ROCK is one of the proteins that regulate membrane changes that may facilitate endocytic processes, membrane blebbing, vesicle formation and release, and the reassembly of the cell cytoskeleton that allows for cell movement, and phagocytosis [15,66–68]. Therefore, ROCK inhibition may lead to alterations in the incorporation of the α-synuclein DNA plasmids over time, thus leading to lower dimer and oligomer formation and lower fluorescence intensity in our experiments [44,45]. However, we eliminated this confusion factor because the ROCK inhibitors were administered 48 h after transfection. AngII exacerbated the activity of the ROCK pathway, leading to a higher number of HMC3 microglial cells showing inclusions and a higher average inclusion size, which was blocked by fasudil. This is consistent with previous studies showing that inhibition of ROCK in microglial cells reduces the engulfment of neuronal debris and inhibits most microglial pro-inflammatory properties, such as the increase in cell body size, number of filopodial processes, and size of Golgi apparatus [10,68]. Interestingly, during neuron apoptosis α-synuclein aggregates are released to the extracellular space, and these aggregates are phagocytosed by microglia, inducing further microglial pro-inflammatory activation [69,70], which would be reduced by ROCK inhibition. However, additional mechanisms may be involved in the decrease in α-synuclein aggregation induced by ROCK inhibition in our cultures of neuronal or glial or HEK293 cells.

Previous studies have shown that oxidative stress, particularly that promoted by NADPH-oxidase activation and its release of superoxide, induces α-synuclein aggregation into oligomers [46–48,71]. Furthermore, NADPH-oxidase-derived oxidative stress is enhanced by superoxide interaction with mitochondria, via mitochondrial ATP-sensitive potassium channels (mitoKATP), leading to further increase in cell ROS levels, as shown in several cell types, including dopaminergic neurons [72,73]. A second interesting factor promoting α-synuclein aggregation is the increase in intracellular free calcium [52], and both oxidative stress and calcium interact to synergistically increase α-synuclein aggregation [47]. It has been observed that the increase in calcium alone led to non-stable aggregates, whereas calcium combined with oxidative stress produced larger and more stable aggregates [51,52]. It has also been observed that, conversely, α-synuclein aggregation increases calcium levels and oxidative stress [74,75], which may lead to further progression of the aggregation process.

In a recent study, we have shown that AngII/AT1 receptor activation increases α-synuclein aggregation, and that this was mediated by an AngII-induced increase in NADPH-oxidase activity and intracellular calcium levels [23]. It is known that there is a mutual interaction between AngII/AT1 and RhoA/ROCK pathways, so AngII-induced NADPH-oxidase activation increases ROCK activity, and ROCK activation further promotes NADPH-oxidase activation [76–78]. AngII/AT1 activation also induces a persistent cytosolic calcium increase in neurons and glial cells [53–55]. The present results show that similar interactions happen regarding α-synuclein aggregation. We observed that the ROCK inhibition with fasudil blocked the increase in α-synuclein aggregation induced by AngII treatment, and also the increase in aggregation observed in the absence of AngII stimulation (e.g. HEK293). Both fasudil and the ROCK inhibitor Y27632 blocked the increase in ROCK activity and NADPH-oxidase activity induced by treatment with AngII or by α-synuclein overexpression, further supporting the involvement of ROCK inhibition and NADPH-oxidase inhibition in the inhibitory effects of fasudil on α-synuclein aggregation [16]. Furthermore, several studies showed that the increase in intracellular calcium levels leads to the activation of RhoA and ROCK, and ROCK activation in turn leads to higher calcium sensitivity, further contributing to a self-perpetuating cycle [79,80].

In cells, accumulation of aggregates may also be related to decreased clearance mechanisms such as autophagy. There are conflicting results regarding ROCK and autophagy. Several studies have observed that ROCK inhibition, particularly fasudil, increased autophagy [81,82]. Conversely, other authors observed that higher ROCK activity led to higher cell autophagy [17,83]. In the present study, we studied the possible effect of changes in autophagy in our results, and we observed that treatment with the ROCK inhibitors fasudil or Y27632 induced a significant increase in autophagy in HMC3 cells overexpressing α-synuclein. This increase in autophagy may therefore contribute to fasudil-induced reduction in α-synuclein aggregates. In our experimental model, fasudil induced a tendency to reduce levels of α-synuclein expression in neuronal, microglial, and HEK293 cells (see Fig. 3a–d), although the decrease was not statistically significant. This suggests that fasudil-induced autophagy was insufficient to significantly reduce the high levels of α-synuclein expression induced by our transfections. However, ROCK inhibition also down-regulates several aforementioned mechanisms that play major roles in promoting α-synuclein aggregation, and the fasudil-induced increase in autophagy may contribute, together with these factors, to the significant decrease in the number and size of aggregates observed in the present study. Consistent with this, a similar effect is observed in the case of treatment with Angiotensin II (see Fig. 3a–d), which did not increase significantly the already high levels of α-synuclein induced by transfections in this model, and in the present and previous studies [23] AngII treatment induced significant increase α-synuclein aggregates, which supports the above-suggested interpretation on the effect of autophagy.

In conclusion, the present results further support that fasudil is an interesting neuroprotective drug against PD progression. In addition to other neuroprotective properties, such as inhibition of neuroinflammation, fasudil inhibits α-synuclein aggregation and microglial endocytosis of aggregates, which enhances the microglial inflammatory response. The effects of fasudil are mostly related to ROCK inhibition, which we have shown using two structurally different ROCK inhibitors and knockdown data, and it is further supported by using real-time quaking-inducing conversion (RT-QuiC). ROCK inhibition down-regulates several factors that promote α-synuclein aggregation such as NADPH-oxidase-derived oxidative stress and intracellular calcium increase, inhibits α-synuclein endocytosis in microglia, and promotes autophagy. Altogether, these mechanisms may contribute to different degrees to the reduction of α-synuclein aggregates, and future work will be needed to elucidate the detailed mechanism. Additional experiments using different methodologies and experimental conditions could provide further insights and reveal other possible downstream effectors of ROCK inhibition.

Availability of data and materials

All data generated or analyzed during this study are included in this published article and its supplementary information files. The datasets produced during the current study can be also available from the corresponding author on reasonable request.

Ethics approval and consent to participate

The protocol of this study involving animals was reviewed and approved by the Ethics Committee of the University of Santiago de Compostela and Galician Government. Project title: Studies of new therapies in models of Parkinson's disease and other neurodegenerative diseases. Approval number: 15012/2021/012 (Last revision: April 16, 2021).

Consent for publication

Not applicable.

Author contributions

LL and ADM performed cell cultures and *in vitro* experiments. AIR-P performed immunohistochemistry and *in vivo* experiments with mice, supervised statistics, and manuscript edition. AD-M and JLL-G conceived and supervised the whole study and wrote the manuscript. All authors read and approved the final manuscript.

Funding

This work was supported by the Spanish Ministry of Science and Innovation (PID2021-126848NB-I00; PLEC2022-009401; PID2023-150743OB-I00), Instituto de Salud Carlos III (RD21/0017/0031 and CIBERNED), Galician Government (XUGA, ED431C 2022/41) and FEDER (Regional European Development Fund).

Declaration of competing interest

The authors declare that they have no known competing financial interests or personal relationships that could have appeared to influence the work reported in this paper.

Acknowledgments

We thank Pilar Aldrey, Iria Novoa, and Cristina Gianzo for their technical assistance. We thank Dr. Tiago Outeiro for donating the original plasmids.

Appendix A. Supplementary data

Supplementary data to this article can be found online at https://doi.org/10.1016/j.neurot.2025.e00544.

References

[1] Feigin VL, Vos T. Global burden of neurological disorders: from global burden of disease estimates to actions. Neuroepidemiology 2019;52(1-2):1–2.
[2] Marras C, Beck JC, Bower JH, Roberts E, Ritz B, Ross GW, et al. Prevalence of Parkinson's disease across North America. NPJ Parkinsons Dis 2018;4:21.
[3] Kouli A, Torsney KM, Kuan WL. Parkinson's disease: etiology, neuropathology, and pathogenesis. In: Stoker TB, Greenland JC, editors. Parkinson's disease: pathogenesis and clinical aspects brisbane (AU); 2018.
[4] Spillantini MG, Schmidt ML, Lee VM, Trojanowski JQ, Jakes R, Goedert M. Alpha-synuclein in Lewy bodies. Nature 1997;388(6645):839–40.
[5] Bendor JT, Logan TP, Edwards RH. The function of alpha-synuclein. Neuron 2013;79(6):1044–66.
[6] He S, Wang F, Yung KKL, Zhang S, Qu S. Effects of alpha-synuclein-associated post-translational modifications in Parkinson's disease. ACS Chem Neurosci 2021;12(7):1061–71.
[7] Davidson WS, Jonas A, Clayton DF, George JM. Stabilization of alpha-synuclein secondary structure upon binding to synthetic membranes. J Biol Chem 1998;273(16):9443–9.
[8] Leung T, Chen XQ, Manser E, Lim L. The p160 RhoA-binding kinase ROK alpha is a member of a kinase family and is involved in the reorganization of the cytoskeleton. Mol Cell Biol 1996;16(10):5313–27.
[9] Matsui T, Amano M, Yamamoto T, Chihara K, Nakafuku M, Ito M, et al. Rho-associated kinase, a novel serine/threonine kinase, as a putative target for small GTP binding protein Rho. EMBO J 1996;15(9):2208–16.
[10] Barcia G, Fleming MR, Deligniere A, Gazula VR, Brown MR, Langouet M, et al. De novo gain-of-function KCNT1 channel mutations cause malignant migrating partial seizures of infancy. Nat Genet 2012;44(11):1255–9.
[11] Borrajo A, Rodriguez-Perez AI, Villar-Cheda B, Guerra MJ, Labandeira-Garcia JL. Inhibition of the microglial response is essential for the neuroprotective effects of Rho-kinase inhibitors on MPTP-induced dopaminergic cell death. Neuropharmacology 2014;85:1–8.
[12] Tonges L, Frank T, Tatenhorst L, Saal KA, Koch JC, Szego EM, et al. Inhibition of rho kinase enhances survival of dopaminergic neurons and attenuates axonal loss in a mouse model of Parkinson's disease. Brain 2012;135(Pt 11):3355–70.
[13] Villar-Cheda B, Dominguez-Meijide A, Joglar B, Rodriguez-Perez AI, Guerra MJ, Labandeira-Garcia JL. Involvement of microglial RhoA/Rho-kinase pathway activation in the dopaminergic neuron death. Role of angiotensin via angiotensin type 1 receptors. Neurobiol Dis 2012;47(2):268–79.
[14] Koch JC, Tatenhorst L, Roser AE, Saal KA, Tonges L, Lingor P. ROCK inhibition in models of neurodegeneration and its potential for clinical translation. Pharmacol Ther 2018;189:1–21.
[15] Labandeira-Garcia JL, Rodriguez-Perez AI, Villar-Cheda B, Borrajo A, Dominguez-Meijide A, Guerra MJ. Rho kinase and dopaminergic degeneration: a promising therapeutic target for Parkinson's disease. Neuroscientist 2015;21(6):616–29.
[16] Hou L, Bao X, Zang C, Yang H, Sun F, Che Y, et al. Integrin CD11b mediates alpha-synuclein-induced activation of NADPH oxidase through a Rho-dependent pathway. Redox Biol 2018;14:600–8.
[17] Iyer M, Subramaniam MD, Venkatesan D, Cho SG, Ryding M, Meyer M, et al. Role of RhoA-ROCK signaling in Parkinson's disease. Eur J Pharmacol 2021;894:173815.
[18] Robustelli P, Ibanez-de-Opakua A, Campbell-Bezat C, Giordanetto F, Becker S, Zweckstetter M, et al. Molecular basis of small-molecule binding to alpha-synuclein. J Am Chem Soc 2022;144(6):2501–10.
[19] Tatenhorst L, Eckermann K, Dambeck V, Fonseca-Ornelas L, Walle H, Lopes da Fonseca T, et al. Fasudil attenuates aggregation of alpha-synuclein in models of Parkinson's disease. Acta Neuropathol Commun 2016;4:39.
[20] Lopez-Lopez A, Labandeira CM, Labandeira-Garcia JL, Munoz A. Rho kinase inhibitor fasudil reduces l-DOPA-induced dyskinesia in a rat model of Parkinson's disease. Br J Pharmacol 2020;177(24):5622–41.
[21] Koch JC, Kuttler J, Maass F, Lengenfeld T, Zielke E, Bahr M, et al. Compassionate use of the ROCK inhibitor fasudil in three patients with amyotrophic lateral sclerosis. Front Neurol 2020;11:173.
[22] Wolff AW, Bidner H, Remane Y, Zimmer J, Aarsland D, Rascol O, et al. Protocol for a randomized, placebo-controlled, double-blind phase IIa study of the safety, tolerability, and symptomatic efficacy of the ROCK-inhibitor Fasudil in patients with Parkinson's disease (ROCK-PD). Front Aging Neurosci 2024;16:1308577.
[23] Lage L, Rodriguez-Perez AI, Villar-Cheda B, Labandeira-Garcia JL, Dominguez-Meijide A. Angiotensin type 1 receptor activation promotes neuronal and glial alpha-synuclein aggregation and transmission. NPJ Parkinsons Dis 2024;10(1):37.
[24] Gibrat C, Saint-Pierre M, Bousquet M, Levesque D, Rouillard C, Cicchetti F. Differences between subacute and chronic MPTP mice models: investigation of dopaminergic neuronal degeneration and alpha-synuclein inclusions. J Neurochem 2009;109(5):1469–82.
[25] Jethva PN, Kardani JR, Roy I. Modulation of alpha-synuclein aggregation by dopamine in the presence of MPTP and its metabolite. FEBS J 2011;278(10):1688–98.
[26] de Los Milagros Bassani Molinas M, Beer C, Hesse F, Wirth M, Wagner R. Optimizing the transient transfection process of HEK-293 suspension cells for protein production by nucleotide ratio monitoring. Cytotechnology 2014;66(3):493–514.
[27] Rivas-Santisteban R, Rodriguez-Perez AI, Munoz A, Reyes-Resina I, Labandeira-Garcia JL, Navarro G, et al. Angiotensin AT(1) and AT(2) receptor heteromer expression in the hemilesioned rat model of Parkinson's disease that increases with levodopa-induced dyskinesia. J Neuroinflammation 2020;17(1):243.
[28] Dominguez-Meijide A, Parrales V, Vasili E, Gonzalez-Lizarraga F, Konig A, Lazaro DF, et al. Doxycycline inhibits alpha-synuclein-associated pathologies in vitro and in vivo. Neurobiol Dis 2021;151:105256.
[29] Santos CC, Cardim-Pires TR, Shvachiy L, Fonseca-Fonseca LA, Munoz P, Almeida A, et al. JM-20, a benzodiazepine-dihydropyridine hybrid molecule, inhibits the formation of alpha-synuclein-aggregated species. Neurotox Res 2022;40(6):2135–47.
[30] Wu JZ, Ardah M, Haikal C, Svanbergsson A, Diepenbroek M, Vaikath NN, et al. Dihydromyricetin and Salvianolic acid B inhibit alpha-synuclein aggregation and enhance chaperone-mediated autophagy. Transl Neurodegener 2019;8:18.
[31] McLean PJ, Kawamata H, Hyman BT. Alpha-synuclein-enhanced green fluorescent protein fusion proteins form proteasome sensitive inclusions in primary neurons. Neuroscience 2001;104(3):901–12.
[32] Giampa M, Amundarain MJ, Herrera MG, Tonali N, Dodero VI. Implementing complementary approaches to shape the mechanism of alpha-synuclein oligomerization as a model of amyloid aggregation. Molecules 2021;27(1).
[33] Masaracchia C, Konig A, Valiente-Gabioud AA, Peralta P, Favretto F, Strohaker T, et al. Molecular characterization of an aggregation-prone variant of alpha-synuclein

used to model synucleinopathies. Biochim Biophys Acta Proteins Proteom 2020; 1868(1):140298.
[34] Dedmon MM, Lindorff-Larsen K, Christodoulou J, Vendruscolo M, Dobson CM. Mapping long-range interactions in alpha-synuclein using spin-label NMR and ensemble molecular dynamics simulations. J Am Chem Soc 2005;127(2):476–7.
[35] Vasili E, Dominguez-Meijide A, Flores-Leon M, Al-Azzani M, Kanellidi A, Melki R, et al. Endogenous levels of alpha-synuclein modulate seeding and aggregation in cultured cells. Mol Neurobiol 2022;59(2):1273–84.
[36] Pernis AB, Ricker E, Weng CH, Rozo C, Yi W. Rho kinases in autoimmune diseases. Annu Rev Med 2016;67:355–74.
[37] Fares MB, Maco B, Oueslati A, Rockenstein E, Ninkina N, Buchman VL, et al. Induction of de novo alpha-synuclein fibrillization in a neuronal model for Parkinson's disease. Proc Natl Acad Sci U S A 2016;113(7):E912–21.
[38] Polinski NK, Volpicelli-Daley LA, Sortwell CE, Luk KC, Cremades N, Gottler LM, et al. Best practices for generating and using alpha-synuclein pre-formed fibrils to model Parkinson's disease in rodents. J Parkinsons Dis 2018;8(2):303–22.
[39] Volpicelli-Daley LA, Luk KC, Lee VM. Addition of exogenous alpha-synuclein preformed fibrils to primary neuronal cultures to seed recruitment of endogenous alpha-synuclein to Lewy body and Lewy neurite-like aggregates. Nat Protoc 2014; 9(9):2135–46.
[40] Sackin H. Hypothesis for renin-angiotensin inhibitor mitigation of COVID-19. Med Hypotheses 2021;152:110609.
[41] Kawahata I, Finkelstein DI, Fukunaga K. Pathogenic impact of alpha-synuclein phosphorylation and its kinases in alpha-synucleinopathies. Int J Mol Sci 2022; 23(11).
[42] Semenyuk PI. REMD simulations of full-length alpha-synuclein together with ligands reveal binding region and effect on amyloid conversion. Int J Mol Sci 2022; 23(19).
[43] Kural MH, Djakbarova U, Chan ET, Madraki Y, Niklason L, Kural C. Mechanoinhibition of endocytosis sensitizes cancer cells to Fas-induced apoptosis. Biophysical Journal 2023;122:514a.
[44] Mao QY, He SY, Hu QY, Lu Y, Niu YX, Li XY, et al. Advanced glycation end products (AGEs) inhibit macrophage efferocytosis of apoptotic beta cells through binding to the receptor for AGEs. J Immunol 2022;208(5):1204–13.
[45] Wayt J, Cartagena-Rivera A, Dutta D, Donaldson JG, Waterman CM. Myosin II isoforms promote internalization of spatially distinct clathrin-independent endocytosis cargoes through modulation of cortical tension downstream of ROCK2. Mol Biol Cell 2021;32(3):226–36.
[46] Cheng SY, Trombetta LD. The induction of amyloid precursor protein and alpha-synuclein in rat hippocampal astrocytes by diethyldithiocarbamate and copper with or without glutathione. Toxicol Lett 2004;146(2):139–49.
[47] Goodwin J, Nath S, Engelborghs Y, Pountney DL. Raised calcium and oxidative stress cooperatively promote alpha-synuclein aggregate formation. Neurochem Int 2013;62(5):703–11.
[48] Musgrove RE, Helwig M, Bae EJ, Aboutalebi H, Lee SJ, Ulusoy A, et al. Oxidative stress in vagal neurons promotes parkinsonian pathology and intercellular alpha-synuclein transfer. J Clin Invest 2019;129(9):3738–53.
[49] Joglar B, Rodriguez-Pallares J, Rodriguez-Perez AI, Rey P, Guerra MJ, Labandeira-Garcia JL. The inflammatory response in the MPTP model of Parkinson's disease is mediated by brain angiotensin: relevance to progression of the disease. J Neurochem 2009;109(2):656–69.
[50] Rodriguez-Pallares J, Rey P, Parga JA, Munoz A, Guerra MJ, Labandeira-Garcia JL. Brain angiotensin enhances dopaminergic cell death via microglial activation and NADPH-derived ROS. Neurobiol Dis 2008;31(1):58–73.
[51] Nath S, Goodwin J, Engelborghs Y, Pountney DL. Raised calcium promotes alpha-synuclein aggregate formation. Mol Cell Neurosci 2011;46(2):516–26.
[52] Rcom-H'cheo-Gauthier AN, Osborne SL, Meedeniya AC, Pountney DL. Calcium: alpha-synuclein interactions in alpha-synucleinopathies. Front Neurosci 2016;10:570.
[53] Gebke E, Muller AR, Jurzak M, Gerstberger R. Angiotensin II-induced calcium signalling in neurons and astrocytes of rat circumventricular organs. Neuroscience 1998;85(2):509–20.
[54] Izumisawa Y, Tanaka-Yamamoto K, Ciriello J, Kitamura N, Shibuya I. Persistent cytosolic Ca(2+) increase induced by angiotensin II at nanomolar concentrations in acutely dissociated subfornical organ (SFO) neurons of rats. Brain Res 2019;1718: 137–47.
[55] Wang D, Martens JR, Posner P, Sumners C, Gelband CH. Angiotensin II regulation of intracellular calcium in astroglia cultured from rat hypothalamus and brainstem. J Neurochem 1996;67(3):996–1004.
[56] Mizushima N, Yoshimori T. How to interpret LC3 immunoblotting. Autophagy 2007;3(6):542–5.
[57] Dominguez-Meijide A, Rodriguez-Perez AI, Diaz-Ruiz C, Guerra MJ, Labandeira-Garcia JL. Dopamine modulates astroglial and microglial activity via glial renin-angiotensin system in cultures. Brain Behav Immun 2017;62:277–90.
[58] Stornetta RL, Hawelu-Johnson CL, Guyenet PG, Lynch KR. Astrocytes s ynthesize angiotensinogen in brain. Science 1988;242(4884):1444–6.
[59] Anderson JP, Walker DE, Goldstein JM, de Laat R, Banducci K, Caccavello RJ, et al. Phosphorylation of Ser-129 is the dominant pathological modification of alpha-synuclein in familial and sporadic Lewy body disease. J Biol Chem 2006;281(40): 29739–52.
[60] Edelman AM, Higgins DM, Bowman CL, Haber SN, Rabin RA, Cho-Lee J. Myosin light chain kinase is expressed in neurons and glia: immunoblotting and immunocytochemical studies. Brain Res Mol Brain Res 1992;14(1-2):27–34.
[61] Li L, Wu X, Yue HY, Zhu YC, Xu J. Myosin light chain kinase facilitates endocytosis of synaptic vesicles at hippocampal boutons. J Neurochem 2016;138(1):60–73.
[62] Solecki DJ, Trivedi N, Govek EE, Kerekes RA, Gleason SS, Hatten ME. Myosin II motors and F-actin dynamics drive the coordinated movement of the centrosome and soma during CNS glial-guided neuronal migration. Neuron 2009;63(1):63–80.
[63] Thomas MG, Santa Coloma TA, Correale J, Boccaci GL. Myosin light chain kinase inhibitors induce retraction of mature oligodendrocyte processes. Neurochem Res 2002;27(11):1305–12.
[64] Yasui Y, Amano M, Nagata K, Inagaki N, Nakamura H, Saya H, et al. Roles of Rho-associated kinase in cytokinesis; mutations in Rho-associated kinase phosphorylation sites impair cytokinetic segregation of glial filaments. J Cell Biol 1998;143(5):1249–58.
[65] Lopez-Lopez A, Villar-Cheda B, Quijano A, Garrido-Gil P, Garcia-Garrote M, Diaz-Ruiz C, et al. NADPH-oxidase, rho-kinase and autophagy mediate the (Pro)renin-Induced pro-inflammatory microglial response and enhancement of dopaminergic neuron death. Antioxidants (Basel) 2021;10(9).
[66] Choi I, Zhang Y, Seegobin SP, Pruvost M, Wang Q, Purtell K, et al. Microglia clear neuron-released alpha-synuclein via selective autophagy and prevent neurodegeneration. Nat Commun 2020;11(1):1386.
[67] Fu P, Tang R, Yu Z, Li C, Chen X, Xie M, et al. Rho-associated kinase inhibitors promote microglial uptake via the ERK signaling pathway. Neurosci Bull 2016; 32(1):83–91.
[68] Scheiblich H, Bicker G. Regulation of microglial phagocytosis by RhoA/ROCK-inhibiting drugs. Cell Mol Neurobiol 2017;37(3):461–73.
[69] He Q, Li YH, Guo SS, Wang Y, Lin W, Zhang Q, et al. Inhibition of Rho-kinase by Fasudil protects dopamine neurons and attenuates inflammatory response in an intranasal lipopolysaccharide-mediated Parkinson's model. Eur J Neurosci 2016; 43(1):41–52.
[70] Zhang W, Wang T, Pei Z, Miller DS, Wu X, Block ML, et al. Aggregated alpha-synuclein activates microglia: a process leading to disease progression in Parkinson's disease. FASEB J 2005;19(6):533–42.
[71] Cristovao AC, Guhathakurta S, Bok E, Je G, Yoo SD, Choi DH, et al. NADPH oxidase 1 mediates alpha-synucleinopathy in Parkinson's disease. J Neurosci 2012;32(42): 14465–77.
[72] Rodriguez-Pallares J, Parga JA, Joglar B, Guerra MJ, Labandeira-Garcia JL. Mitochondrial ATP-sensitive potassium channels enhance angiotensin-induced oxidative damage and dopaminergic neuron degeneration. Relevance for aging-associated susceptibility to Parkinson's disease. Age (Dordr) 2012;34(4):863–80.
[73] Zawada WM, Banninger GP, Thornton J, Marriott B, Cantu D, Rachubinski AL, et al. Generation of reactive oxygen species in 1-methyl-4-phenylpyridinium (MPP+) treated dopaminergic neurons occurs as an NADPH oxidase-dependent two-wave cascade. J Neuroinflammation 2011;8:129.
[74] Dryanovski DI, Guzman JN, Xie Z, Galteri DJ, Volpicelli-Daley LA, Lee VM, et al. Calcium entry and alpha-synuclein inclusions elevate dendritic mitochondrial oxidant stress in dopaminergic neurons. J Neurosci 2013;33(24):10154–64.
[75] Hettiarachchi NT, Parker A, Dallas ML, Pennington K, Hung CC, Pearson HA, et al. alpha-Synuclein modulation of Ca2+ signaling in human neuroblastoma (SH-SY5Y) cells. J Neurochem 2009;111(5):1192–201.
[76] Bali A, Jaggi AS. An integrative review on role and mechanisms of ghrelin in stress, anxiety and depression. Curr Drug Targets 2016;17(5):495–507.
[77] Lopez-Lopez A, Valenzuela R, Rodriguez-Perez AI, Guerra MJ, Labandeira-Garcia JL, Munoz A. Interactions between angiotensin type-1 antagonists, statins, and ROCK inhibitors in a rat model of L-DOPA-induced dyskinesia. Antioxidants (Basel) 2023;12(7).
[78] Rodriguez-Perez AI, Borrajo A, Rodriguez-Pallares J, Guerra MJ, Labandeira-Garcia JL. Interaction between NADPH-oxidase and Rho-kinase in angiotensin II-induced microglial activation. Glia 2015;63(3):466–82.
[79] Mancini AE, Rizzo MA. A novel single-color FRET sensor for rho-kinase reveals calcium-dependent activation of RhoA and ROCK. Sensors (Basel) 2024;24(21).
[80] Phelps C, Chess-Williams R, Moro C. The role of intracellular calcium and Rho kinase pathways in G protein-coupled receptor-mediated contractions of urinary bladder urothelium and lamina propria. Am J Physiol Cell Physiol 2023;324(3): C787–97.
[81] Liu FT, Yang YJ, Wu JJ, Li S, Tang YL, Zhao J, et al. Fasudil, a Rho kinase inhibitor, promotes the autophagic degradation of A53T alpha-synuclein by activating the JNK 1/Bcl-2/beclin 1 pathway. Brain Res 2016;1632:9–18.
[82] Yan Y, Xiang C, Yang Z, Miao D, Zhang D. Rho kinase inhibition by fasudil attenuates adriamycin-induced chronic. Heart Injury Cardiovasc Toxicol 2020; 20(4):351–60.
[83] Gurkar AU, Chu K, Raj L, Bouley R, Lee SH, Kim YB, et al. Identification of ROCK1 kinase as a critical regulator of Beclin1-mediated autophagy during metabolic stress. Nat Commun 2013;4:2189.